

# MULTI-INDEX ENSEMBLE KALMAN FILTERING

HÅKON HOEL, GAUKHAR SHAIMERDENOVA\*, AND RAÚL TEMPONE

**ABSTRACT.** In this work we marry multi-index Monte Carlo with ensemble Kalman filtering (EnKF) to produce the multi-index EnKF method (MIEnKF). The MIEnKF method is based on independent samples of four-coupled EnKF estimators on a multi-index hierarchy of resolution levels, and it may be viewed as an extension of the multilevel EnKF (MLEnKF) method developed by the same authors in 2020. Multi-index here refers to a two-index method, consisting of a hierarchy of EnKF estimators that are coupled in two degrees of freedom: time discretization and ensemble size. Under certain assumptions, the MIEnKF method is proven to be more tractable than EnKF and MLEnKF, and this is also verified in numerical examples.

**Key words:** Monte Carlo, multilevel, multi-index, convergence rates, Kalman filter, ensemble Kalman filter

**AMS subject classification:** 65C30, 65Y20.

## 1. INTRODUCTION

The ensemble Kalman filtering (EnKF) method is a widely used data assimilation method for high-dimensional state-space problems with nonlinear dynamics. Owing to its simple implementation and efficiency, ensemble-based filtering methods have rapidly gained popularity in geophysical sciences with applications, for example, in weather forecasting [37], atmosphere-ocean/lake simulations [34, 6, 28], and oil reservoir management [1, 52]. The EnKF method was originally proposed by Evensen [17]. Subsequently, several variants were developed [33, 13, 3]. EnKF approximates the filtering distribution using the empirical measure of its ensemble members. The  $L^p$ -convergence of the EnKF method with perturbed observations [33] has been studied in the literature [45, 42].

A challenge in numerical ensemble-based data assimilation is the significant increase in the numerical simulation cost with an increase in temporal resolution. This challenge can be overcome using the Monte Carlo method (MLMC) [21], which achieves a substantial reduction in variance by simulating pairwise-coupled realizations on a hierarchy of temporal discretization levels. MLMC is an extremely flexible method that has been combined with other methods and successfully implemented in various fields; for instance, the quasi-Monte Carlo [22, 40, 51], sequential Monte Carlo [11, 10, 47, 41], inverse problems and experimental design [9, 53, 43, 23, 54], differential equations with randomness [36, 16, 7, 39, 8, 4], limit theorems [2, 30], importance sampling [29, 38, 18], and machine learning [44].

The multilevel EnKF (MLEnKF) method was introduced by Hoel et al. [31] for stochastic differential equation models with discrete-time observations, and an alternative version based on a sample average of independent pairwise-coupled EnKF estimators was subsequently developed [32]. The main difference between these two

---

\*Corresponding author: G.Shaimerdenova (gaukhar.shaimerdenova@kaust.edu.sa).

versions of MLEnKF is that the first version [31] uses one universal Kalman gain to update the ensemble members on all hierarchy levels, while the second version [32] employs one Kalman gain per independent EnKF sample in the full MLEnKF estimator. The latter approach introduces less correlation between all particle members of the MLEnKF estimator, which particularly simplifies convergence analysis and paves the way for extending MLEnKF to the multi-index EnKF (MIEnKF) method introduced in this work. The MLEnKF method was extended to spatiotemporal (infinite-dimensional state space) models [15]. Similar multilevel techniques were combined with other ensemble-based filtering methods; examples of such combinations are particle filtering [35, 5], transform particle filtering [25, 24], multigrid [46] and the recent extension to continuous-time (Kalman–Bucy) filtering [14].

The successful implementation of MLMC depends on a strong pairwise coupling of realizations on neighboring hierarchy levels. Achieving such a coupling for stochastic differential equations with sufficiently smooth coefficients is relatively straightforward (once the idea is introduced). However, in more realistic problems with low-regularity features, strong coupling can be extremely challenging, if at all possible. An assessment of MLEnKF in reservoir history matching [19] and for applications using sampling resolution constraints (the so-called multi-fidelity methods) [20, 49, 50] are described in the literature.

Another important method is the multi-index Monte Carlo method (MIMC) [26], which forms the basis of this work. MIMC consists of a multi-index hierarchy of coupled realizations on neighboring resolutions, and can be regarded as an extension of MLMC. Many concepts related to particle-wise coupling in the proposed MIEnKF method are common in the MIMC method for McKean-Vlasov dynamics [27].

The main contribution of this work is to develop the MIEnKF method as an extension of the MLEnKF by treating both the numerical discretization and EnKF ensemble size as degrees of freedom. The extension introduces four coupled of EnKF estimators (i.e., a coupling in both degrees of freedom) yielding a stronger variance reduction than that achieved by pairwise-coupling in MLEnKF. Under certain assumptions, this approach achieves efficiency gains (Table 1) for computing the weak approximations of quantities of interest (QoI).

Methods	EnKF	MLEnKF	MIEnKF
Mean-squared error	$\mathcal{O}(\epsilon^2)$	$\mathcal{O}(\epsilon^2)$	$\mathcal{O}(\epsilon^2)$
Computational cost	$\mathcal{O}(\epsilon^{-3})$	$\mathcal{O}(\epsilon^{-2}  \log(\epsilon) ^3)$	$\mathcal{O}(\epsilon^{-2})$

TABLE 1. Comparison of computational costs versus errors for ensemble Kalman filtering (EnKF), multilevel EnKF (MLEnKF) and multi-index EnKF (MIEnKF) methods, cf. Section 4.

The rest of this work is organized as follows. In Section 2, the setting and notation for filtering problem are introduced and a brief overview of the EnKF, mean-field EnKF (MFEEnKF), and MLEnKF methods is presented. In Section 3, the MIEnKF algorithm is provided. The main theorem of MIEnKF complexity is presented in Section 4. In Section 5, a numerical comparison of filtering algorithms is provided. The concluding remarks are presented in Section 6.

## 2. PROBLEM SETTING

In this section, the problem setting and basic notation commonly used in data assimilation are introduced and the EnKF, MFEnKF and MLEnKF methods are briefly reviewed.

Let  $(\Omega, \mathcal{F}, \mathbb{P}; \{\mathcal{F}_t\}_{t \geq 0})$  be a complete probability space equipped with a filtration  $\{\mathcal{F}_t\}_{t \geq 0}$  of sub- $\sigma$ -algebras of  $\mathcal{F} = \mathcal{F}_\infty$ . We denote by  $L_t^p(\Omega, \mathbb{R}^k)$  the space of  $\mathcal{F}_t \setminus \mathcal{B}^k$ -measurable functions<sup>1</sup>  $u : \Omega \rightarrow \mathbb{R}^k$  with  $\mathbb{E}[|u|^p] < \infty$ . Given the initial value  $u_0 \in \cap_{p \geq 2} L_0^p(\Omega, \mathbb{R}^d)$ , we consider the discrete-time filtering problem for a system of stochastic dynamics defined by a sequence of random maps  $\Psi_n : \mathbb{R}^d \times \Omega \rightarrow \mathbb{R}^d$  and observations with additive noise:

$$\begin{cases} u_{n+1}(\omega) = \Psi_n(u_n, \omega), \\ y_{n+1}(\omega) = H u_{n+1}(\omega) + \eta_{n+1}, \end{cases}$$

where  $\omega \in \Omega$ ,  $n \in \mathbb{N}_0$ ,  $H \in \mathbb{R}^{m \times d}$  is an observation operator,  $\{\eta_k\}_{k \in \mathbb{N}}$  is an independent and identically distributed (i.i.d) sequence with  $\eta_1 \sim N(0, \Gamma)$ . Hereinafter, we do not indicate the dependence on  $\omega$  for ease of notation, whenever there is no confusion. Let  $Y_n := (y_1, y_2, \dots, y_n)$  denote the accumulated observation data up to time  $n$  with the convention  $Y_0 := \emptyset$ . The main objective of a filtering method is to track the underlying signal  $u_n$  for given  $Y_n$  by computing the (filtering) distribution of the conditional random variable  $u_n | Y_n$ . The Bayesian interpretation of the filtering problem can be expressed formally using the following iterative steps for computing the filtering density:

$$\textbf{Prediction} \quad \rho_{u_n | Y_{n-1}}(u) \propto \int_{\mathbb{R}^d} \rho_{u_n | u_{n-1}}(u) \rho_{u_{n-1} | Y_{n-1}}(v) dv$$

$$\textbf{Update} \quad \rho_{u_n | Y_n}(u) \propto \exp\left(-|\Gamma^{-1/2}(y_n - Hu)|^2/2\right) \rho_{u_n | Y_{n-1}}(u),$$

In the linear Gaussian setting, the exact filter distribution is provided in a closed form using the Kalman filter, however, when  $\Psi$  is nonlinear, the filter distribution must be approximated. Hence, we construct an efficient MLEnKF method that converges weakly to the mean-field EnKF in the large-ensemble limit. In other words, for a given QoI  $\varphi : \mathbb{R}^d \rightarrow \mathbb{R}$ , our method approximates

$$\mathbb{E}^{\bar{\mu}_n}[\varphi(u)] = \int_{\mathbb{R}^d} \varphi(u) \bar{\mu}_n(du),$$

where  $\bar{\mu}_n$  denotes the mean-field EnKF measure at time  $n$ , cf. Section 2.2.

**Notation.**

- For  $f, g : (0, \infty) \rightarrow [0, \infty)$  the notation  $f \lesssim g$  implies that there exists a  $C > 0$  such that

$$f(x) \leq Cg(x), \quad \forall x \in (0, \infty).$$

- The notation  $f \approx g$  implies that  $f \lesssim g$  and  $g \lesssim f$ .
- For  $d \in \mathbb{N}$ ,  $|x|$  denotes the Euclidean norm of a vector  $x \in \mathbb{R}^d$ . For  $\mathcal{F} \setminus \mathcal{B}^d$ -measurable functions  $u : \Omega \rightarrow \mathbb{R}^d$  and  $p \geq 1$ ,

$$\|u\|_p := \|u\|_{L^p(\Omega, \mathbb{R}^d)} = \left( \int_{\Omega} |u(\omega)|^p \mathbb{P}(d\omega) \right)^{1/p}.$$

<sup>1</sup>The function  $u$  is  $\mathcal{F}_t \setminus \mathcal{B}^k$ -measurable iff  $u^{-1}(B) \in \mathcal{F}_t$  for all  $B \in \mathcal{B}^k$ , where  $\mathcal{B}^k$  is the Borel  $\sigma$ -algebra on  $\mathbb{R}^k$ .

- $\lceil x \rceil := \min\{z \in \mathbb{Z} \mid z \geq x\}$ .

We denote by  $\Psi_n^N$  the numerical discretization of the dynamics  $\Psi_n$  using  $N \geq 1$  uniform timesteps, and we consider that the following assumptions are satisfied:

**Assumption 1.** *Let  $u, v \in \cap_{p \geq 2} L_n^p(\Omega, \mathbb{R}^d)$  for any  $n \in \mathbb{N}_0$ ,  $p \geq 2$ . Given that  $\varphi$  is Lipschitz, there exists a constant  $c_p > 0$  such that for all  $N \geq 1$ :*

- (i)  $\|\Psi_n^N(u)\|_p \leq c_p(1 + \|u\|_p)$ ,
- (ii)  $\|\Psi_n^N(u) - \Psi_n^N(v)\|_p < c_p \|u - v\|_p$ .

**Remark 1.** *Assumption 1 is mainly introduced so that it ensures the existence of the mean-field EnKF measure  $\bar{\mu}_n$ , cf. [32, Appendix A] and Section 2.2.*

**2.1. EnKF.** The EnKF method is an ensemble-based extension of the Kalman filter to nonlinear settings. For an EnKF ensemble of size  $P$ , let  $v_{n,i} := v_n(\omega_i)$  and  $\hat{v}_{n,i} := \hat{v}_n(\omega_i)$ , respectively, denote the  $i$ -th particle of the prediction and updated ensemble at time  $n$ . Then, the EnKF algorithm with perturbed observations and numerical dynamics  $\Psi^N$  comprises the following steps:

$$\begin{aligned} \text{Prediction} & \begin{cases} v_{n+1,i} = \Psi_n^N(\hat{v}_{n,i}), & i = 1, 2, \dots, P, \\ m_{n+1} = \frac{1}{P} \sum_{i=1}^P v_{n+1,i}, \\ C_{n+1} = \frac{1}{P-1} \sum_{i=1}^P (v_{n+1,i} - m_{n+1})(v_{n+1,i} - m_{n+1})^{\mathbf{T}}. \end{cases} \\ \text{Update} & \begin{cases} \tilde{y}_{n+1,i} = y_{n+1} + \eta_{n+1,i}, & i = 1, 2, \dots, P, \\ K_{n+1} = C_{n+1} H^{\mathbf{T}} (H C_{n+1} H^{\mathbf{T}} + \Gamma)^{-1}, \\ \hat{v}_{n+1,i} = (I - K_{n+1} H) v_{n+1,i} + K_{n+1} \tilde{y}_{n+1,i}, \end{cases} \end{aligned}$$

where  $\eta_{n+1,i}$  are i.i.d. draws from  $N(0, \Gamma)$ .

The updated EnKF empirical measure is defined by

$$\mu_n^{N,P}(dv) = \frac{1}{P} \sum_{i=1}^P \delta(dv; \hat{v}_{n,i}),$$

where  $\delta$  is the Dirac measure centered at  $\hat{v}_{n,i}$ , and the expectation of a QoI  $\varphi : \mathbb{R}^d \rightarrow \mathbb{R}$  with respect to the EnKF empirical measure is expressed as

$$(1) \quad \mu_n^{N,P}[\varphi] = \frac{1}{P} \sum_{i=1}^P \varphi(\hat{v}_{n,i}).$$

Note that  $\mu_n^{N,P}[\varphi]$  is a random variable that depends on parameters  $N$  and  $P$ . Under sufficient regularity,  $\mu_n^{N,P}[\varphi] \rightarrow \bar{\mu}_n[\varphi]$  as  $N, P \rightarrow \infty$ , where  $\bar{\mu}_n[\varphi]$  denotes the known as the expectation of  $\varphi$  with respect to the mean-field EnKF measure (Section 2.2).

**2.2. MFEnKF.** The MFEnKF is the large-ensemble and fine-discretization limit of EnKF. In the large-ensemble limit, the Kalman gain becomes a deterministic matrix. Consequently, one may view MFEnKF as an ensemble of i.i.d. noninteracting particles, so that it suffices to represent the resulting filtering distribution by one particle. Let  $\bar{v}_n$  and  $\hat{\bar{v}}_n$  denote the prediction and updated state of a mean-field

particle at time  $n$ , respectively. The following algorithm defines the MFEnKF for fully non-Gaussian models:

$$\begin{aligned} \text{Prediction} & \begin{cases} \bar{v}_{n+1} = \Psi_n(\hat{v}_n) \\ \bar{m}_{n+1} = \mathbb{E}[\hat{v}_{n+1}], \\ \bar{C}_{n+1} = \mathbb{E}\left[(\hat{v}_{n+1} - \bar{m}_{n+1})(\hat{v}_{n+1} - \bar{m}_{n+1})^{\mathbf{T}}\right]. \end{cases} \\ \text{Update} & \begin{cases} \tilde{y}_{n+1} = y_{n+1} + \tilde{\eta}_{n+1}, \\ \bar{K}_{n+1} = \bar{C}_{n+1}H^{\mathbf{T}}(H\bar{C}_{n+1}H^{\mathbf{T}} + \Gamma)^{-1}, \\ \hat{v}_{n+1,i} = (I - \bar{K}_{n+1}H)\hat{v}_{n+1,i} + \bar{K}_{n+1}\tilde{y}_{n+1,i}, \end{cases} \end{aligned}$$

where  $\tilde{\eta}_{n+1}$  is i.i.d. draws from  $N(0, \Gamma)$ .

The expectation of a QoI  $\varphi : \mathbb{R}^d \rightarrow \mathbb{R}$  with respect to the updated mean-field EnKF measure is given by

$$\bar{\mu}_n[\varphi] = \int_{\mathbb{R}^d} \varphi(v) \bar{\mu}_n(dv).$$

**2.3. MLEnKF.** The recently developed MLEnKF algorithm [32] is a natural stepping stone en route from EnKF to MIEnKF, for gradually adding layers to the EnKF notation. MLEnKF is a filtering method based on a sample average of independent and pairwise-coupled samples of EnKF estimators at different resolution levels. Let  $L \in \mathbb{N}$  denote the finest resolution level of the estimator, let the sequences

$$N_\ell = N_0 \times 2^\ell \quad \text{and} \quad P_\ell = P_0 \times 2^\ell \quad \text{with} \quad N_0, P_0 \in \mathbb{N}$$

denote the numerical resolution and ensemble size on level  $\ell$ , respectively. Then, the updated MLEnKF estimator at time  $n$  assumes the following form:

$$(2) \quad \mu_n^{ML}[\varphi] = \sum_{\ell=0}^L \sum_{m=1}^{M_\ell} \frac{\left( \mu_n^{N_\ell, P_\ell, m} - (\mu_n^{N_{\ell-1}, P_{\ell-1}, 1, m} + \mu_n^{N_{\ell-1}, P_{\ell-1}, 2, m})/2 \right) [\varphi]}{M_\ell}$$

where  $\{M_\ell\}_{\ell=0}^L \subset \mathbb{N}$  is a decreasing sequence with  $M_\ell$  representing the number of i.i.d. and pairwise-coupled EnKF estimators

$$\left\{ \mu_n^{N_\ell, P_\ell, m}[\varphi], (\mu_n^{N_{\ell-1}, P_{\ell-1}, 1, m}[\varphi], \mu_n^{N_{\ell-1}, P_{\ell-1}, 2, m}[\varphi]) \right\}_{m=1}^{M_\ell}$$

on level  $\ell$ , and  $\mu_n^{N_{-1}, P_{-1}, m}[\varphi] := 0$ .

*Pairwise coupling of EnKF estimators.* For  $\ell \geq 1$ , let

$$\hat{v}_{n,i}^\ell := \hat{v}_n^\ell(\omega_i) \quad i = 1, \dots, P_\ell$$

denote an updated ensemble at time  $n$  coupled to the following two coarser-level updated ensembles:

$$\hat{v}_{n,i}^{\ell-1,1} := \hat{v}_n^{\ell-1,1}(\omega_i) \quad i = 1, \dots, P_{\ell-1}$$

and

$$\hat{v}_{n,i}^{\ell-1,2} := \hat{v}_n^{\ell-1,2}(\omega_{P_{\ell-1}+i}) \quad i = 1, \dots, P_{\ell-1}.$$

The coupling is imposed under the particle-wise shared initial condition:

$$\hat{v}_{0,i}^\ell = \begin{cases} \hat{v}_{0,i}^{\ell-1,1} & \text{if } i \in \{1, \dots, P_{\ell-1}\} \\ \hat{v}_{0,i-P_{\ell-1}}^{\ell-1,2} & \text{if } i \in \{P_{\ell-1} + 1, \dots, P_\ell\}, \end{cases}$$

and using the following prediction and update steps, where the driving noise and the perturbed observations are also shared particle wise:

$$\text{Prediction} \begin{cases} v_{n+1,i}^{\ell-1,1} = \Psi_n^{N_{\ell-1}}(\hat{v}_{n,i}^{\ell-1,1}), & i = 1, \dots, P_{\ell-1}, \\ v_{n+1,i}^{\ell-1,2} = \Psi_n^{N_{\ell-1}}(\hat{v}_{n,i}^{\ell-1,2}), & i = 1, \dots, P_{\ell-1}, \\ v_{n+1,i}^{\ell} = \Psi_n^{N_{\ell}}(\hat{v}_{n,i}^{\ell}), & i = 1, \dots, P_{\ell}, \\ C_{n+1}^{\ell-1,1} = \overline{\text{Cov}}[v_{n+1,1:P_{\ell-1}}^{\ell-1,1}], \\ C_{n+1}^{\ell-1,2} = \overline{\text{Cov}}[v_{n+1,1:P_{\ell-1}}^{\ell-1,2}], \\ C_{n+1}^{\ell} = \overline{\text{Cov}}[v_{n+1,1:P_{\ell}}^{\ell}], \end{cases}$$

$$\overline{\text{Cov}}[v_{n,1:P_{\ell}}^{\ell}] := \sum_{i=1}^{P_{\ell}} \frac{v_{n,i}^{\ell}(v_{n,i}^{\ell})^{\mathbf{T}}}{P_{\ell}} - \sum_{i=1}^{P_{\ell}} \frac{v_{n,i}^{\ell}}{P_{\ell}} \left( \sum_{i=1}^{P_{\ell}} \frac{v_{n,i}^{\ell}}{P_{\ell}} \right)^{\mathbf{T}},$$

$$\overline{\text{Cov}}[v_{n,1:P_{\ell-1}}^{\ell-1,k}] := \sum_{i=1}^{P_{\ell-1}} \frac{v_{n,i}^{\ell-1,k}(v_{n,i}^{\ell-1,k})^{\mathbf{T}}}{P_{\ell-1}} - \sum_{i=1}^{P_{\ell-1}} \frac{v_{n,i}^{\ell-1,k}}{P_{\ell-1}} \left( \sum_{i=1}^{P_{\ell-1}} \frac{v_{n,i}^{\ell-1,k}}{P_{\ell-1}} \right)^{\mathbf{T}}, \quad k = 1, 2.$$

$$\text{Update} \begin{cases} \tilde{y}_{n+1,i}^{\ell} = y_{n+1} + \eta_{n+1,i}^{\ell}, & i = 1, \dots, P_{\ell}, \\ K_{n+1}^{\ell-1,1} = C_{n+1}^{\ell-1,1} H^{\mathbf{T}} (H C_{n+1}^{\ell-1,1} H^{\mathbf{T}} + \Gamma)^{-1}, \\ K_{n+1}^{\ell-1,2} = C_{n+1}^{\ell-1,2} H^{\mathbf{T}} (H C_{n+1}^{\ell-1,2} H^{\mathbf{T}} + \Gamma)^{-1}, \\ K_{n+1}^{\ell} = C_{n+1}^{\ell} H^{\mathbf{T}} (H C_{n+1}^{\ell} H^{\mathbf{T}} + \Gamma)^{-1}, \\ \hat{v}_{n+1,i}^{\ell-1,1} = (I - K_{n+1}^{\ell-1,1} H) v_{n+1,i}^{\ell-1,1} + K_{n+1}^{\ell-1,1} \tilde{y}_{n+1,i}^{\ell}, & i = 1, \dots, P_{\ell-1}, \\ \hat{v}_{n+1,i}^{\ell-1,2} = (I - K_{n+1}^{\ell-1,2} H) v_{n+1,i}^{\ell-1,2} + K_{n+1}^{\ell-1,2} \tilde{y}_{n+1,P_{\ell-1}+i}^{\ell}, & i = 1, \dots, P_{\ell-1}, \\ \hat{v}_{n+1,i}^{\ell} = (I - K_{n+1}^{\ell} H) v_{n+1,i}^{\ell} + K_{n+1}^{\ell} \tilde{y}_{n+1,i}^{\ell}, & i = 1, \dots, P_{\ell}, \end{cases}$$

where  $\{\eta_{n+1,i}^{\ell}\}_{i=1}^{P_{\ell}}$  is a sequence of independent  $N(0, \Gamma)$ -distributed random variables. In the above notation, the coupling between the fine-level EnKF estimator

$$\mu_n^{N_{\ell}, P_{\ell}}[\varphi] := \sum_{i=1}^{P_{\ell}} \frac{\varphi(\hat{v}_{n,i}^{\ell})}{P_{\ell}},$$

and the two coarse-level estimators

$$\mu_n^{N_{\ell-1}, P_{\ell-1}, k}[\varphi] := \sum_{i=1}^{P_{\ell-1}} \frac{\varphi(\hat{v}_{n,i}^{\ell-1,k})}{P_{\ell-1}}, \quad k = 1, 2$$

is obtained through particle-wise coupling

$$\hat{v}_{n,i}^{\ell} \xleftrightarrow{\text{coupling}} \begin{cases} \hat{v}_{n,i}^{\ell-1,1} & \text{if } i \in \{1, \dots, P_{\ell-1}\}, \\ \hat{v}_{n,i-P_{\ell-1}}^{\ell-1,2} & \text{if } i \in \{P_{\ell-1} + 1, \dots, P_{\ell}\}. \end{cases}$$

### 3. MIENKF

This section describes the MIEnKF method by extending the MLEnKF method in Section 2.3.

To define a set of multi-index discretizations for the MIEnKF, we first introduce  $\ell := (\ell_1, \ell_2) \in \mathbb{N}_0^2$  and shorthands  $\mathbf{e}_1 := (1, 0)$ ,  $\mathbf{e}_2 := (0, 1)$ , and  $\mathbf{1} := (1, 1)$ .

Similarly for MLEnKF, we associate sequences of natural numbers  $N_{\ell_1} = N_0 \times 2^{\ell_1}$  and  $P_{\ell_2} = P_0 \times 2^{\ell_2}$  to the number of timesteps and particles on the 2-index “level”  $\ell$ .

We seek to approximate the mean-field measure  $\bar{\mu}_n[\varphi]$  and we denote the discrete approximation corresponding to the 2-index  $\ell$  by  $\mu_n^\ell[\varphi] := \mu_n^{N_{\ell_1}, P_{\ell_2}}[\varphi]$ . In other words,  $\mu_n^\ell[\varphi]$  is the EnKF estimator (1) computed using  $N_{\ell_1}$  timesteps and  $P_{\ell_2}$  particles. We define first-order difference operators for numbers of timesteps and particles as follows:

$$(3) \quad \begin{aligned} \Delta_1 \mu_n^\ell[\varphi] &= \begin{cases} (\mu_n^\ell - \mu_n^{\ell-e_1})[\varphi], & \text{if } \ell_1 > 0, \\ \mu_n^\ell[\varphi], & \text{if } \ell_1 = 0 \end{cases} \\ \Delta_2 \mu_n^\ell[\varphi] &= \begin{cases} (\mu_n^\ell - (\mu_n^{\ell-e_2,1} + \mu_n^{\ell-e_2,2})/2)[\varphi], & \text{if } \ell_2 > 0, \\ \mu_n^\ell[\varphi], & \text{if } \ell_2 = 0 \end{cases} \end{aligned}$$

where  $\mu_n^{\ell-e_2,1}[\varphi]$  and  $\mu_n^{\ell-e_2,2}[\varphi]$  are two i.i.d. copies of  $\mu_n^{\ell-e_2}[\varphi]$ . Note that  $\mu_n^\ell[\varphi]$  comprises  $P_{\ell_2}$  ensemble members, whereas  $\mu_n^{\ell-e_2}[\varphi]$  consists of  $P_{\ell_2-1}$ , i.e., half as many ensemble members. Therefore, the pair  $(\mu_n^{\ell-e_2,1}[\varphi], \mu_n^{\ell-e_2,2}[\varphi])$  are introduced to uniquely couple each ensemble member from  $\mu_n^\ell[\varphi]$  with one from the “level”  $\ell - e_2$ .

We define the four-coupled EnKF estimator using the first-order mixed difference as follows:

$$(4) \quad \begin{aligned} \Delta \mu_n^\ell[\varphi] &:= \Delta_1(\Delta_2 \mu_n^\ell[\varphi]) = \Delta_2(\Delta_1 \mu_n^\ell[\varphi]) = \Delta_2(\mu_n^\ell - \mu_n^{\ell-e_1})[\varphi] \\ &= \left( \mu_n^\ell - (\mu_n^{\ell-e_2,1} + \mu_n^{\ell-e_2,2})/2 \right. \\ &\quad \left. - \mu_n^{\ell-e_1} + (\mu_n^{\ell-1,1} + \mu_n^{\ell-1,2})/2 \right)[\varphi], \end{aligned}$$

where the pair  $(\mu_n^{\ell-1,1}[\varphi], \mu_n^{\ell-1,2}[\varphi])$  of i.i.d. copies of  $\mu_n^{\ell-1}[\varphi]$  is also introduced to uniquely couple  $\mu_n^\ell[\varphi]$  with one from the “level”  $\ell - 1$ . Under the assumption that  $\mathbb{E}[\mu_n^\ell[\varphi]] \rightarrow \bar{\mu}_n[\varphi]$  as  $|\ell| \rightarrow \infty$ , the linearity of the expectation operator implies that

$$(5) \quad \bar{\mu}_n[\varphi] = \sum_{\ell \in \mathbb{N}_0^2} \mathbb{E}[\Delta \mu_n^\ell[\varphi]] = \sum_{\ell \in \mathcal{I}} \mathbb{E}[\Delta \mu_n^\ell[\varphi]] + \sum_{\ell \notin \mathcal{I}} \mathbb{E}[\Delta \mu_n^\ell[\varphi]],$$

for any index set  $\mathcal{I} \subset \mathbb{N}_0^2$ .

For a properly selected index set  $\mathcal{I}$ , which we will specify later (Section 4), the MIEnKF estimator is defined as the sample-average estimator of the first term on the right-hand side of (5):

$$(6) \quad \mu_n^{MI}[\varphi] := \sum_{\ell \in \mathcal{I}} \sum_{m=1}^{M_\ell} \frac{\Delta \mu_n^{\ell,m}[\varphi]}{M_\ell},$$

where  $\{\Delta \mu_n^{\ell,m}[\varphi]\}_{m=1}^{M_\ell}$  are i.i.d. copies of  $\Delta \mu_n^{\ell,m}[\varphi]$ , and  $\{\Delta \mu_n^{\ell,m}[\varphi]\}_{(\ell,m)}$  are mutually independent.

The primary motivation for sampling four-coupled EnKF estimators in the MIEnKF estimator is that the coupling may lead to a substantial variance reduction, thus

improving the efficiency of the sampling method. Similar to the setting of multi-level Monte Carlo estimators, the tractability of (6) is optimized through careful selection of the index set  $\mathcal{I}$  and the number of samples  $M_\ell$ . This can be achieved by solving a constrained optimization problem using the knapsack algorithm [26, 27].

*Four-coupled EnKF estimators.* To describe the coupling between the EnKF estimators  $(\mu_n^\ell, \mu_n^{\ell-e_2}, \mu_n^{\ell-e_1}, \mu_n^{\ell-1})[\varphi]$ , we introduce the four-coupled updated-state ensembles  $\{(\hat{v}_n^\ell, \hat{v}_n^{\ell-e_2}, \hat{v}_n^{\ell-e_1}, \hat{v}_n^{\ell-1})_i\}_{i=1}^{P_{\ell_2}}$ . The second ensemble of particles is a union of two EnKF ensembles:

$$\hat{v}_{n,i}^{\ell-e_2,1} := \hat{v}_{n,i}^{\ell-e_2} \quad i = 1, \dots, P_{\ell_2-1},$$

and

$$\hat{v}_{n,i}^{\ell-e_2,2} := \hat{v}_{n,P_{\ell_2-1}+i}^{\ell-e_2} \quad i = 1, \dots, P_{\ell_2-1},$$

and the fourth ensemble is also a union of two EnKF ensembles:

$$\hat{v}_{n,i}^{\ell-1,1} := \hat{v}_{n,i}^{\ell-1} \quad i = 1, \dots, P_{\ell_2-1},$$

and

$$\hat{v}_{n,i}^{\ell-1,2} := \hat{v}_{n,P_{\ell_2-1}+i}^{\ell-1} \quad i = 1, \dots, P_{\ell_2-1}.$$

Further details regarding the nature of the particle-wise four-coupling of these ensembles is provided in Section 3.1.

The empirical estimator  $\mu_n^\ell[\varphi]$  is induced by the ensemble  $\hat{v}_{n,1:P_{\ell_2}}^\ell := \{\hat{v}_{n,i}^\ell\}_{i=1}^{P_{\ell_2}}$ , meaning that it equals the sample average of  $\{\varphi(\hat{v}_{n,i}^\ell)\}_{i=1}^{P_{\ell_2}}$ . Similarly,  $\mu_n^{\ell-e_1}[\varphi]$  is induced by  $\hat{v}_{n,1:P_{\ell_2}}^{\ell-e_1} := \{\hat{v}_{n,i}^{\ell-e_1}\}_{i=1}^{P_{\ell_2}}$ ,

$$\mu_n^{\ell-e_2}[\varphi] := \frac{(\mu_n^{\ell-e_2,1} + \mu_n^{\ell-e_2,2})[\varphi]}{2}$$

is induced by the union of two ensembles

$$\hat{v}_{n,1:P_{\ell_2}}^{\ell-e_2} := \{\hat{v}_{n,k}^{\ell-e_2,1}\}_{k=1}^{P_{\ell_2-1}} \cup \{\hat{v}_{n,k}^{\ell-e_2,2}\}_{k=1}^{P_{\ell_2-1}},$$

and

$$\mu_n^{\ell-1}[\varphi] := \frac{(\mu_n^{\ell-1,1} + \mu_n^{\ell-1,2})[\varphi]}{2}$$

is induced by  $\hat{v}_{n,1:P_{\ell_2}}^{\ell-1} := \{\hat{v}_{n,k}^{\ell-1,1}\}_{k=1}^{P_{\ell_2-1}} \cup \{\hat{v}_{n,k}^{\ell-1,2}\}_{k=1}^{P_{\ell_2-1}}$ . For consistency with (3), we impose the condition that  $\mu_n^{\ell-e_1}[\varphi] = \mu_n^{\ell-1}[\varphi] = 0$  when  $\ell_1 = 0$ , and  $\mu_n^{\ell-e_2}[\varphi] = 0$  when  $\ell_2 = 0$ . Figure 1 shows a visual description of all the couplings of the MIEnKF estimator.

Then, the MIEnKF estimator (6) can also be written as

$$(7) \quad \mu_n^{MI}[\varphi] := \sum_{\ell \in \mathcal{I}} \sum_{m=1}^{M_\ell} \frac{(\mu_n^{\ell,m} - \mu_n^{\ell-e_1,m} - \mu_n^{\ell-e_2,m} + \mu_n^{\ell-1,m})[\varphi]}{M_\ell}$$

where  $\{(\mu_n^{\ell,m}, \mu_n^{\ell-e_1,m}, \mu_n^{\ell-e_2,m}, \mu_n^{\ell-1,m})[\varphi]\}_m$  are independent copies of the estimators  $(\mu_n^\ell, \mu_n^{\ell-e_1}, \mu_n^{\ell-e_2}, \mu_n^{\ell-1})[\varphi]$  and  $\{(\mu_n^{\ell,m}, \mu_n^{\ell-e_1,m}, \mu_n^{\ell-e_2,m}, \mu_n^{\ell-1,m})[\varphi]\}_{(\ell,m)}$  are mutually independent.



**Remark 2.** For comparison, one can also represent the MLEnKF estimator (2) using the above 2-index notation

$$\mu_n^{ML}[\varphi] = \sum_{\ell=0}^L \sum_{m=1}^{M_\ell} \frac{(\mu_n^{(\ell,\ell),m} - (\mu_n^{(\ell,\ell)-1,m})[\varphi])}{M_\ell}.$$

**3.1. Particle-wise four-coupling for MIEnKF.** We now describe how the four-coupling of EnKF estimators manifests itself on the particle level. At time  $n = 0$ , the fine-index update ensemble  $\{\hat{v}_{0,i}^\ell\}_{i=1}^{P_{\ell_2}}$  comprises independent  $\mathbb{P}_{u_0|Y_0}$ -distributed samples that are particle-wise coupled to three other ensembles as

$$\hat{v}_{0,i}^\ell = \hat{v}_{0,i}^{\ell-e_1} = \hat{v}_{0,i}^{\ell-e_2} = \hat{v}_{0,i}^{\ell-1} \quad \text{for } i = 1, 2, \dots, P_{\ell_2}.$$

Given the four-coupled updated states  $(\hat{v}_{n,i}^\ell, \hat{v}_{n,i}^{\ell-e_1}, \hat{v}_{n,i}^{\ell-e_2}, \hat{v}_{n,i}^{\ell-1})$  at some  $n \geq 0$ , their next-time prediction states are computed using the dynamics

$$\begin{aligned} v_{n+1,i}^\ell &= \Psi_n^{N_{\ell_1}}(\hat{v}_{n,i}^\ell), & v_{n+1,i}^{\ell-e_1} &= \Psi_n^{N_{\ell_1-1}}(\hat{v}_{n,i}^{\ell-e_1}), \\ v_{n+1,i}^{\ell-e_2} &= \Psi_n^{N_{\ell_1}}(\hat{v}_{n,i}^{\ell-e_2}), & v_{n+1,i}^{\ell-1} &= \Psi_n^{N_{\ell_1-1}}(\hat{v}_{n,i}^{\ell-1}), \end{aligned}$$

where the four particles share the same driving noise. The sample covariance matrices and Kalman gains are expressed as follows:

$$\begin{aligned} C_{n+1}^\ell &= \overline{\text{Cov}}[v_{n+1}^\ell], & K_{n+1}^\ell &= C_{n+1}^\ell H^\mathbf{T} (H C_{n+1}^\ell H^\mathbf{T} + \Gamma)^{-1}, \\ C_{n+1}^{\ell-e_1} &= \overline{\text{Cov}}[v_{n+1}^{\ell-e_1}], & K_{n+1}^{\ell-e_1} &= C_{n+1}^{\ell-e_1} H^\mathbf{T} (H C_{n+1}^{\ell-e_1} H^\mathbf{T} + \Gamma)^{-1}, \end{aligned}$$

and

$$\begin{aligned} C_{n+1}^{\ell-e_2,1} &= \overline{\text{Cov}}[v_{n+1}^{\ell-e_2,1}], & K_{n+1}^{\ell-e_2,1} &= C_{n+1}^{\ell-e_2,1} H^\mathbf{T} (H C_{n+1}^{\ell-e_2,1} H^\mathbf{T} + \Gamma)^{-1}, \\ C_{n+1}^{\ell-e_2,2} &= \overline{\text{Cov}}[v_{n+1}^{\ell-e_2,2}], & K_{n+1}^{\ell-e_2,2} &= C_{n+1}^{\ell-e_2,2} H^\mathbf{T} (H C_{n+1}^{\ell-e_2,2} H^\mathbf{T} + \Gamma)^{-1}, \\ C_{n+1}^{\ell-1,1} &= \overline{\text{Cov}}[v_{n+1}^{\ell-1,1}], & K_{n+1}^{\ell-1,1} &= C_{n+1}^{\ell-1,1} H^\mathbf{T} (H C_{n+1}^{\ell-1,1} H^\mathbf{T} + \Gamma)^{-1}, \\ C_{n+1}^{\ell-1,2} &= \overline{\text{Cov}}[v_{n+1}^{\ell-1,2}], & K_{n+1}^{\ell-1,2} &= C_{n+1}^{\ell-1,2} H^\mathbf{T} (H C_{n+1}^{\ell-1,2} H^\mathbf{T} + \Gamma)^{-1}. \end{aligned}$$

The perturbed observations are also particle-wise coupled, so that one obtains the updated particle states:

$$(8) \quad \left. \begin{aligned} \tilde{y}_{n+1,i}^\ell &= y_{n+1} + \eta_{n+1,i}^\ell, \\ \hat{v}_{n+1,i}^\ell &= (I - K_{n+1}^\ell H) v_{n+1,i}^\ell + K_{n+1}^\ell \tilde{y}_{n+1,i}^\ell, \\ \hat{v}_{n+1,i}^{\ell-e_1} &= (I - K_{n+1}^{\ell-e_1} H) v_{n+1,i}^{\ell-e_1} + K_{n+1}^{\ell-e_1} \tilde{y}_{n+1,i}^\ell, \end{aligned} \right\} \quad i = 1, \dots, P_{\ell_2}.$$

$$(9) \quad \left. \begin{aligned} \hat{v}_{n+1,i}^{\ell-e_2,1} &= (I - K_{n+1}^{\ell-e_2,1} H) v_{n+1,i}^{\ell-e_2,1} + K_{n+1}^{\ell-e_2,1} \tilde{y}_{n+1,i}^\ell, \\ \hat{v}_{n+1,i}^{\ell-e_2,2} &= (I - K_{n+1}^{\ell-e_2,2} H) v_{n+1,i}^{\ell-e_2,2} + K_{n+1}^{\ell-e_2,2} \tilde{y}_{n+1,i+P_{\ell_2-1}}^\ell, \\ \hat{v}_{n+1,i}^{\ell-1,1} &= (I - K_{n+1}^{\ell-1,1} H) v_{n+1,i}^{\ell-1,1} + K_{n+1}^{\ell-1,1} \tilde{y}_{n+1,i}^\ell, \\ \hat{v}_{n+1,i}^{\ell-1,2} &= (I - K_{n+1}^{\ell-1,2} H) v_{n+1,i}^{\ell-1,2} + K_{n+1}^{\ell-1,2} \tilde{y}_{n+1,i+P_{\ell_2-1}}^\ell, \end{aligned} \right\} \quad i = 1, \dots, P_{\ell_2-1}.$$

where  $\{\eta_{n+1,i}^{\ell_2}\}_{i=1}^{P_{\ell_2}}$  are i.i.d. with  $\eta_{n+1,1}^{\ell_2} \sim N(0, \Gamma)$ . Thus, the four-coupled ensembles are correlated based on the shared initial condition, driving noise, and perturbed observations.

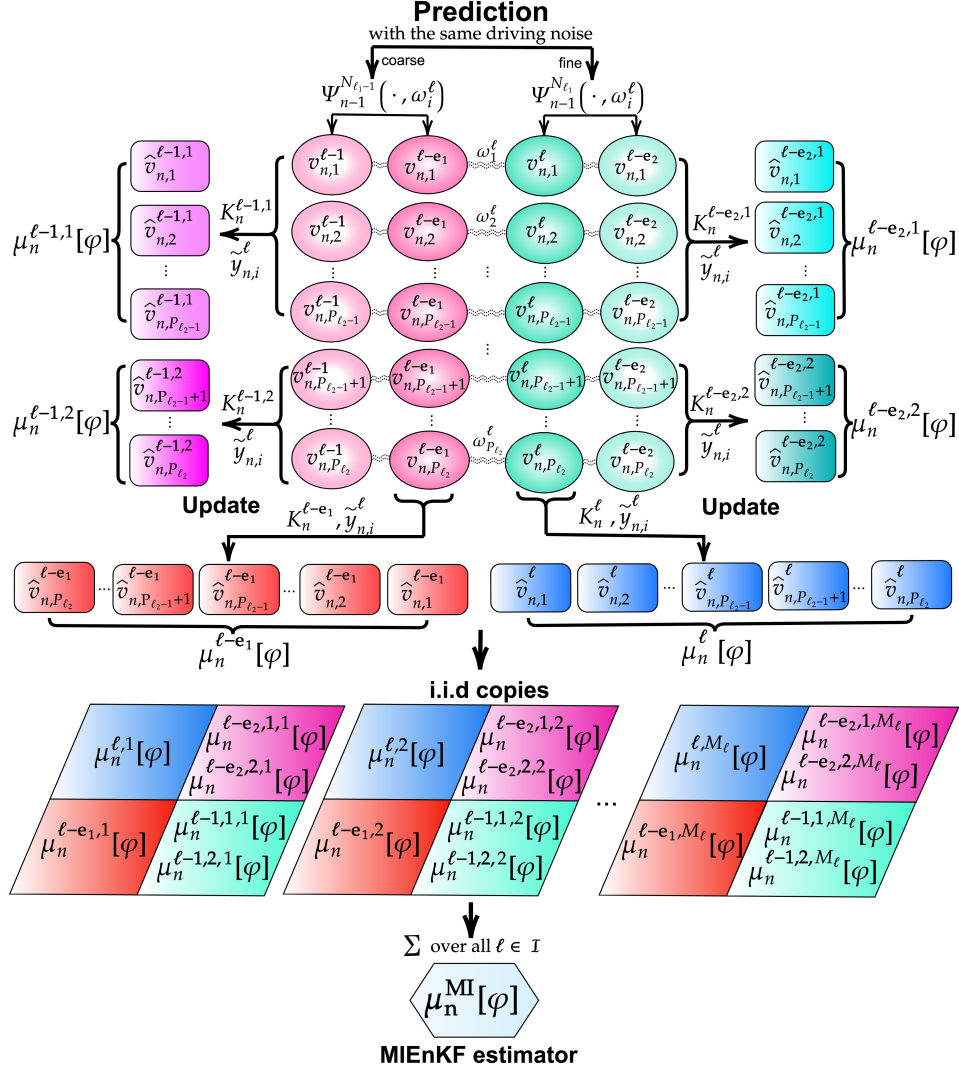


FIGURE 1. One prediction-update iteration of the multi-index ensemble Kalman filtering (MIEnKF) estimator described in Section 3.1. The ovals represent four-coupled prediction-state particles, sharing the same driving noise  $\omega^\ell$  and coupled initial conditions. The respective squares represent updated-state particles sharing the same perturbed observations.

#### 4. MIENKF COMPLEXITY

This section presents a complexity result for MIEnKF and a comparison of MIEnKF, MLEnKF and EnKF in terms of complexity.

**Assumption 2.** For some  $N_0, P_0 \in \mathbb{N}$ ,

$$N_{\ell_1} = N_0 \times 2^{\ell_1} \quad \text{and} \quad P_{\ell_2} = P_0 \times 2^{\ell_2} \quad \forall \ell \in \mathbb{N}_0^2.$$

For any  $\mathcal{B}^d \setminus \mathcal{B}$ -measurable<sup>2</sup> mapping  $\varphi : \mathbb{R}^d \rightarrow \mathbb{R}$  with integrability conditions  $\bar{\mu}_n[\varphi], \mu_n^\ell[\varphi] < \infty$  for any  $n \geq 0$ , the four-coupled EnKF estimator  $\Delta\mu_n^\ell[\varphi]$  satisfies the following assumptions:

$$(A1) \quad |\mathbb{E}[\Delta\mu_n^\ell[\varphi]]| \lesssim N_{\ell_1}^{-1} P_{\ell_2}^{-1},$$

$$(A2) \quad \mathbb{V}[\Delta\mu_n^\ell[\varphi]] \lesssim N_{\ell_1}^{-2} P_{\ell_2}^{-2},$$

and

$$(A3) \quad \text{Cost}(\Delta\mu_n^\ell[\varphi]) \approx N_{\ell_1} P_{\ell_2}.^3$$

**Theorem 1** (MIEnKF complexity). *Let Assumptions 1 and 2 hold and for any  $\epsilon > 0$  consider the MIEnKF estimator with the index set  $\mathcal{I} = \{\ell \in \mathbb{N}_0^2 \mid \ell_1 + \ell_2 \leq L\}$  and*

$$L = \max\left(\lceil \log \epsilon^{-1} + \log \log \epsilon^{-1} \rceil - L_0, 1\right), \quad L_0 \in \mathbb{N}_0,$$

$$M_\ell \approx \epsilon^{-2} N_{\ell_1}^{-3/2} P_{\ell_2}^{-3/2}.$$

Then it holds for any  $n \geq 0$  that

$$(10) \quad \mathbb{E}\left[(\mu_n^{MI}[\varphi] - \bar{\mu}_n[\varphi])^2\right] \lesssim \epsilon^2,$$

and the computational cost of the MIEnKF estimator is bounded by

$$\text{Cost}(\mu_n^{MI}[\varphi]) \approx \epsilon^{-2}.$$

*Proof.* Introducing  $\pm \mathbb{E}[\mu_n^{MI}[\varphi]]$  in the mean-squared error, we obtain

$$\mathbb{E}\left[(\mu_n^{MI}[\varphi] - \bar{\mu}_n[\varphi])^2\right] = \mathbb{V}[\mu_n^{MI}[\varphi]] + (\mathbb{E}[\mu_n^{MI}[\varphi]] - \bar{\mu}_n[\varphi])^2.$$

For the variance term, the independence of the random variables  $\{\Delta\mu_n^{\ell,m}[\varphi]\}_{(\ell,m)}$  and **A2** yield

$$\mathbb{V}[\mu_n^{MI}[\varphi]] = \sum_{\ell \in \mathcal{I}} \sum_{m=1}^{M_\ell} \frac{\mathbb{V}[\Delta\mu_n^{\ell,m}[\varphi]]}{M_\ell} \lesssim \sum_{\ell \in \mathcal{I}} M_\ell^{-1} N_{\ell_1}^{-2} P_{\ell_2}^{-2} \lesssim \epsilon^2.$$

For the squared bias term, **A1** and the multi-index telescoping properties of the MIEnKF estimator imply that

$$(\mathbb{E}[\mu_n^{MI}[\varphi]] - \bar{\mu}_n[\varphi])^2 \leq \left(\sum_{\ell \notin \mathcal{I}} \mathbb{E}[\Delta\mu_n^\ell[\varphi]]\right)^2 \lesssim \left(\sum_{\ell \notin \mathcal{I}} N_{\ell_1}^{-1} P_{\ell_2}^{-1}\right)^2.$$

The mean-squared error bound (10) follows by

$$\sum_{\ell \notin \mathcal{I}} N_{\ell_1}^{-1} P_{\ell_2}^{-1} \lesssim \sum_{\ell_1 + \ell_2 > L} 2^{-(\ell_1 + \ell_2)} = \sum_{k=L+1}^{\infty} (k+1)2^{-k} \approx 2^{-L} L \approx \epsilon$$

and

$$\text{Cost}(\mu_n^{MI}[\varphi]) = \sum_{\ell \in \mathcal{I}} M_\ell \text{Cost}(\Delta\mu_n^\ell[\varphi]) \approx \sum_{\ell \in \mathcal{I}} M_\ell N_{\ell_1} P_{\ell_2} \approx \epsilon^{-2}.$$

□

<sup>2</sup>The mapping  $\varphi$  is  $\mathcal{B}^d \setminus \mathcal{B}$ -measurable iff  $\varphi^{-1}(B) \in \mathcal{B}^d$  for all  $B \in \mathcal{B}$ , where  $\mathcal{B}$  and  $\mathcal{B}^d$  are the  $\sigma$ -algebras on  $\mathbb{R}$  and  $\mathbb{R}^d$ , respectively.

<sup>3</sup>Note that **A3** is the trivial assumption followed from Section 3.1 because the cost of the one prediction-update iteration of the MIEnKF algorithm is linear in  $N_{\ell_1}$  and  $P_{\ell_2}$ .

**Remark 3.** For comparison, we briefly recall the cost-versus-accuracy results for EnKF and MLEnKF. For any  $\epsilon > 0$  and sufficient regularity

$$\|(\mu_n^{N,P} - \bar{\mu}_n)[\varphi]\|_p \lesssim \epsilon, \quad (\text{EnKF})$$

$$\|(\mu_n^{ML} - \bar{\mu}_n)[\varphi]\|_p \lesssim \epsilon, \quad (\text{MLEnKF})$$

with the computational cost bounded by

$$\text{Cost}(\mu_n^{N,P}[\varphi]) \approx \epsilon^{-3},$$

$$\text{Cost}(\mu_n^{ML}[\varphi]) \approx \epsilon^{-2} |\log(\epsilon)|^3.$$

For more details, see [32].

**Remark 4.** An alternative to **A2** that is more aligned with assumption made for the existing convergence results for MLEnKF is to assume that

$$(\mathbf{A2}^*) \quad \|\Delta\mu_n^\ell[\varphi]\|_p \lesssim N_{\ell_1}^{-1} P_{\ell_2}^{-1},$$

for  $p \geq 2$ . Then, using the same aforementioned index set  $\mathcal{I}$  and  $L$  and with a slight change in the sample size  $M_\ell \approx \epsilon^{-2} N_{\ell_1}^{-4/3} P_{\ell_2}^{-4/3}$ , the MIEnKF estimator satisfies

$$(11) \quad \|(\mu_n^{MI} - \bar{\mu}_n)[\varphi]\|_p \lesssim \epsilon,$$

with the asymptotic MIEnKF cost bounded by  $\mathcal{O}(\epsilon^{-2})$ . This can be proved similarly as the case of Theorem 1, where the  $L_p$ -norm of the statistical error can be bounded using the Marcinkiewicz-Zygmund inequality:

$$\begin{aligned} \|(\mu_n^{MI} - \bar{\mu}_n)[\varphi]\|_p &\leq \|\mu_n^{MI}[\varphi] - \mathbb{E}[\mu_n^{MI}][\varphi]\|_p + \|\mathbb{E}[\mu_n^{MI}][\varphi] - \bar{\mu}_n[\varphi]\|_p \\ &\lesssim \sum_{\ell \in \mathcal{I}} M_\ell^{-1/2} \|\Delta\mu_n^{\ell,m}[\varphi]\|_p + \sum_{\ell \notin \mathcal{I}} |\mathbb{E}[\Delta\mu_n^{\ell,m}[\varphi]]|. \end{aligned}$$

We note that **A2** is a weaker assumption than **A2\*** since

$$(12) \quad \mathbb{V}[\Delta\mu_n^\ell[\varphi]] \leq \|\Delta\mu_n^\ell[\varphi]\|_2^2 \leq \|\Delta\mu_n^\ell[\varphi]\|_p^2.$$

**Remark 5.** Under more general settings, Assumption 2 may be transformed into

$$(\mathcal{A}_1) \quad |\mathbb{E}[\Delta\mu_n^\ell[\varphi]]| \lesssim N_{\ell_1}^{-\alpha_1} P_{\ell_2}^{-\alpha_2},$$

$$(\mathcal{A}_2) \quad \|\Delta\mu_n^\ell[\varphi]\|_p \lesssim N_{\ell_1}^{-\beta_1} P_{\ell_2}^{-\beta_2},$$

$$(\mathcal{A}_3) \quad \text{Cost}(\Delta\mu_n^\ell[\varphi]) \approx N_{\ell_1}^{\gamma_1} P_{\ell_2}^{\gamma_2},$$

for some  $\alpha_1, \alpha_2, \beta_1, \beta_2, \gamma_1, \gamma_2 > 0$ . The construction of an efficient MIEnKF estimator may then lead to a differently shaped index set  $\mathcal{I}$  and number of samples  $\{M_\ell\}_\ell$ , and it may even be sensible to consider different common ratios for the geometric sequences  $\{N_{\ell_1}\}$  and  $\{P_{\ell_2}\}$ . The problem of optimizing the set  $\mathcal{I}$  may be recast as a knapsack problem, which is a well-studied optimization problem with many available solution algorithms, cf. [26] and [27, equation (21)].

## 5. NUMERICAL EXAMPLES

This section presents a numerical comparison of MIEnKF with the EnKF and MLEnKF methods outlined in Section 2. Three problems will be considered: the Ornstein-Uhlenbeck (OU) process, a stochastic differential equation (SDE) with a double-well (DW) potential, and Langevin dynamics.

We consider SDE on the general form

$$(13) \quad du = -U'(u)dt + \sigma dW_t,$$

with a constant diffusion coefficient  $\sigma = 0.5$  and two types of potential functions:

$$\begin{aligned} (i) \quad U(u) &= u^2/2, & (\text{OU}) \\ (ii) \quad U(u) &= u^2/4 + 1/(4u^2 + 2), & (\text{DW}). \end{aligned}$$

The numerical discretizations of (13) are computed using the Milstein numerical scheme with uniform timestep  $\Delta t = 1/N$  for any  $N \geq 1$ . The observations of the process  $u$  are equally spaced with observation time interval  $\tau = 1$ , observation operator  $H = 1$ ,  $\Gamma = 0.1$  and the QoI  $\varphi(x) = x$ .

To numerically verify assumptions **A1** and **A2\***, the following rates are estimated from  $S$  independent copies of  $\Delta\mu_n^\ell[\varphi]$ :

$$\begin{aligned} |\mathbb{E}[\Delta\mu_n^\ell[\varphi]]| &\approx \left| \sum_{i=1}^S \frac{\Delta\mu_{n,i}^\ell[\varphi]}{S} \right|, \\ \|\Delta\mu_n^\ell[\varphi]\|_2 &\approx \sqrt{\frac{1}{S} \sum_{i=1}^S |\Delta\mu_{n,i}^\ell[\varphi]|^2}. \end{aligned}$$

We analyze the convergence rates of the methods by computing the time-averaged root-mean-squared error (RMSE).

$$\text{RMSE} := \sqrt{\frac{1}{S(\mathcal{N} + 1)} \sum_{i=1}^S \sum_{n=0}^{\mathcal{N}} |\mu_{n,i}^*[\varphi] - \bar{\mu}_n[\varphi]|^2},$$

where  $\{\mu_{i,n}^*[\varphi]\}_{i=1}^S$  are independent copies of  $\mu^*[\varphi]$  for the specific methods (EnKF, MLEnKF, and MIEnKF).

**5.1. Reference solutions and computer architecture.** Since dynamics  $\Psi$  is linear for the OU problem, the reference solution  $\bar{\mu}_n[\varphi]$  can be computed exactly using the Kalman filter. However, the reference solution for the DW problem, which involves nonlinear dynamics, must be approximated. This solution is computed using the deterministic mean-field EnKF algorithm, cf. [32, Appendix C]. A pseudoreference solution for the final test problem based on Langevin dynamics is computed by the sample average of  $S = 180$  independent simulations of the MIEnKF estimator at the tolerance  $\epsilon = 2^{-11}$  using the following parameters:

$$\begin{aligned} L &= \lceil L_* + \log_2(L_*) \rceil - 1, & \text{with } L_* &= \lceil \log_2(\epsilon^{-1}) \rceil - 1, \\ N_{\ell_1} &= 4 \times 2^{\ell_1}, \\ P_{\ell_2} &= 30 \times 2^{\ell_2}, \\ M_{\ell} &= \begin{cases} 6 \times \lceil \epsilon^{-2} N_{\ell_1}^{-3/2} P_{\ell_2}^{-3/2} \rceil & \text{if } \ell_1 = 0 \text{ and } \ell_2 = 0, \\ 90 \times \lceil \epsilon^{-2} N_{\ell_1}^{-3/2} P_{\ell_2}^{-3/2} \rceil & \text{if } 1 \leq \ell_1 + \ell_2 \leq L. \end{cases} \end{aligned}$$

The numerical simulations were computed in parallel on 18 cores on an Intel(R) Xeon(R) CPU E5-2680 v2 20-core processor with 128 GB RAM. The computer code was written in the Julia programming language [12], and it can be downloaded from <https://github.com/GaukharSH/mienkf>.

**5.2. Ornstein-Uhlenbeck process.** We consider the SDE (13) with the (OU) potential function and initial condition  $u(0) \sim N(0, \Gamma)$ . Convergence rates **A1** and **A2\*** shown in Figure 2 were estimated by the Monte Carlo method using  $S = 10^6$  independent samples of  $\Delta\mu_n^\ell[\varphi]$ . In the figure, the left panel shows the weak and  $L_2$  convergence rates over  $\mathcal{N} = 10$  observation times with  $(\ell_1 + \ell_2) \in [0, 7]$ , and the right panel shows the ratio of the rates to  $N_{\ell_1}^{-1}P_{\ell_2}^{-1}$ . The plane-like flatness of the right panel for  $(\ell_1 + \ell_2) \in [1, 7]$  validates the said rate assumptions.

When conducting runtime-versus-accuracy convergence tests for an input tolerance  $\epsilon > 0$ , we set the parameters of the respective methods as follows:

$$(14) \quad \mathbf{EnKF}: \quad P = \lceil 15\epsilon^{-2} \rceil \quad \text{and} \quad N = \lceil \epsilon^{-1} \rceil,$$

$$(15) \quad \mathbf{MLEnKF}: \quad \begin{cases} L = \lceil \log_2(\epsilon^{-1}) \rceil - 1, \\ N_\ell = 2 \times 2^\ell, \\ P_\ell = 10 \times 2^\ell, \\ M_\ell = \begin{cases} 2 \times \lceil \epsilon^{-2} L^2 2^{-3} \rceil & \text{if } \ell = 0, \\ \lceil \epsilon^{-2} L^2 2^{-2\ell-3} \rceil & \text{if } 1 \leq \ell \leq L, \end{cases} \end{cases}$$

and

$$(16) \quad \mathbf{MIEnKF}: \quad \begin{cases} L = \lceil L_* + \log_2(L_*) \rceil - 1, \quad \text{with } L_* = \lceil \log_2(\epsilon^{-1}) \rceil - 1, \\ N_{\ell_1} = 4 \times 2^{\ell_1}, \\ P_{\ell_2} = 30 \times 2^{\ell_2}, \\ M_\ell = \begin{cases} 6 \times \lceil \epsilon^{-2} N_{\ell_1}^{-3/2} P_{\ell_2}^{-3/2} \rceil & \text{if } \ell_1 = 0 \text{ and } \ell_2 = 0, \\ 120 \times \lceil \epsilon^{-2} N_{\ell_1}^{-3/2} P_{\ell_2}^{-3/2} \rceil & \text{if } 1 \leq \ell_1 + \ell_2 \leq L. \end{cases} \end{cases}$$

For a sequence of predefined tolerances  $\epsilon = [2^{-4}, 2^{-5}, 2^{-6}, 2^{-7}, 2^{-8}, 2^{-9}]$  for EnKF and MLEnKF, and  $\epsilon = [2^{-4}, 2^{-5}, 2^{-6}, 2^{-7}, 2^{-8}, 2^{-9}, 2^{-10}, 2^{-11}]$  for MIEnKF, Figure 3 shows the runtime against the RMSE for the three methods over observation times of  $\mathcal{N} = 10$  and  $\mathcal{N} = 100$  estimated using  $S = 100$  independent runs. MIEnKF outperforms EnKF and MLEnKF for sufficiently small tolerances, and the complexity rate agrees with the theory.

**5.3. Double-well SDE.** We consider the SDE (13) with the DW potential function and  $u(0) \sim N(0, \Gamma)$ . Similar to the OU case, Figure 4 provides numerical evidence of the conjecture rates under assumptions **A1** and **A2\***. For the same predefined  $\epsilon$ -inputs with the same degrees of freedom setting as in the example of OU, the performance of the three methods were compared in terms of runtime against RMSE for observation times  $\mathcal{N} = 10$  and  $\mathcal{N} = 100$  and estimated over  $S = 100$  independent runs (Figure 5). We observe that MIEnKF outperforms EnKF and MLEnKF for small RMSE.

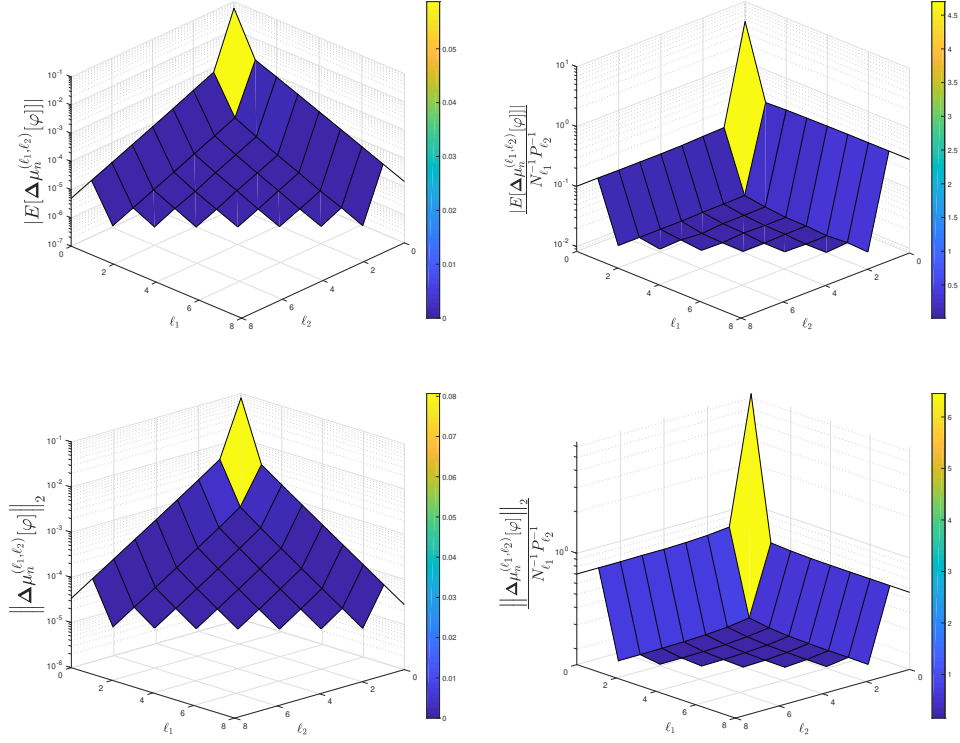


FIGURE 2. **Ornstein-Uhlenbeck problem. Estimates based on  $S = 10^6$  independent runs (Section 5.2).** Top row: Numerical evidence of assumption **A1** over  $\mathcal{N} = 20$  observation times when using  $N_{\ell_1} = 4 \times 2^{\ell_1}$  and  $P_{\ell_2} = 20 \times 2^{\ell_2}$ . Bottom row: Similar plots for the verification of assumption **A2\***.

5.4. **Langevin SDE.** In the last example, we consider the two-dimensional stochastic Langevin dynamics

$$(17) \quad \begin{aligned} dX_t &= V_t dt, \\ dV_t &= -U'(X_t) dt - \kappa V_t dt + (2\kappa T)^{1/2} dW_t, \end{aligned}$$

where  $X_t$  and  $V_t$  denotes the particle position and velocity, respectively,  $U(X)$  is the previously introduced DW potential,  $\kappa = 2^{-5} \times \pi^2$  is the viscosity and  $T = 1$  is the temperature. To improve the pairwise coupling between particles, we used the first-order symplectic Euler splitting scheme [48]. The initial conditions are provided by  $X_0 \sim N(0, \Gamma)$  and  $P_0 \sim N(0, \Gamma)$  with  $X_0$  and  $P_0$  being independent. Further, based on initial test runs, the method parameters are set to

$$\mathbf{EnKF}: \quad P = \lceil 10\epsilon^{-2} \rceil \quad \text{and} \quad N = \lceil \epsilon^{-1} \rceil,$$

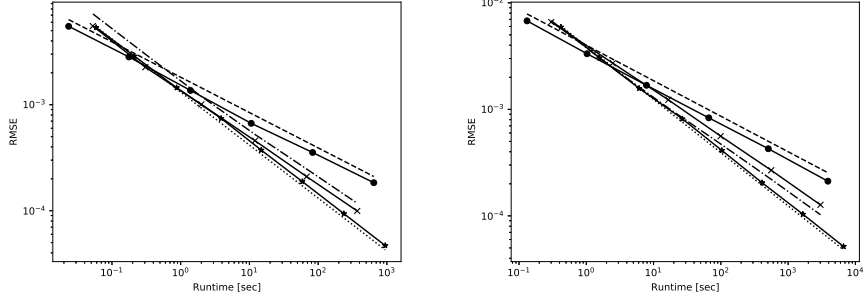


FIGURE 3. **Ornstein-Uhlenbeck problem. Estimates based on  $S = 100$  independent runs (Section 5.2).** Comparison of the runtime versus root-mean-squared error (RMSE) for mean over observation times  $\mathcal{N} = 10$  (left) and  $\mathcal{N} = 100$  (right). The solid-crossed line represents MLEnKF and the dot-dashed line is a fitted  $\mathcal{O}(\log(10 + \text{Runtime})^{1/3} \text{Runtime}^{-1/2})$  reference line. The solid-asterisk line represents the MIEnKF and the dotted line is a fitted  $\mathcal{O}(\text{Runtime}^{-1/2})$  reference line. The solid-bulleted line represents EnKF and the dashed line is a fitted  $\mathcal{O}(\text{Runtime}^{-1/3})$  reference line.

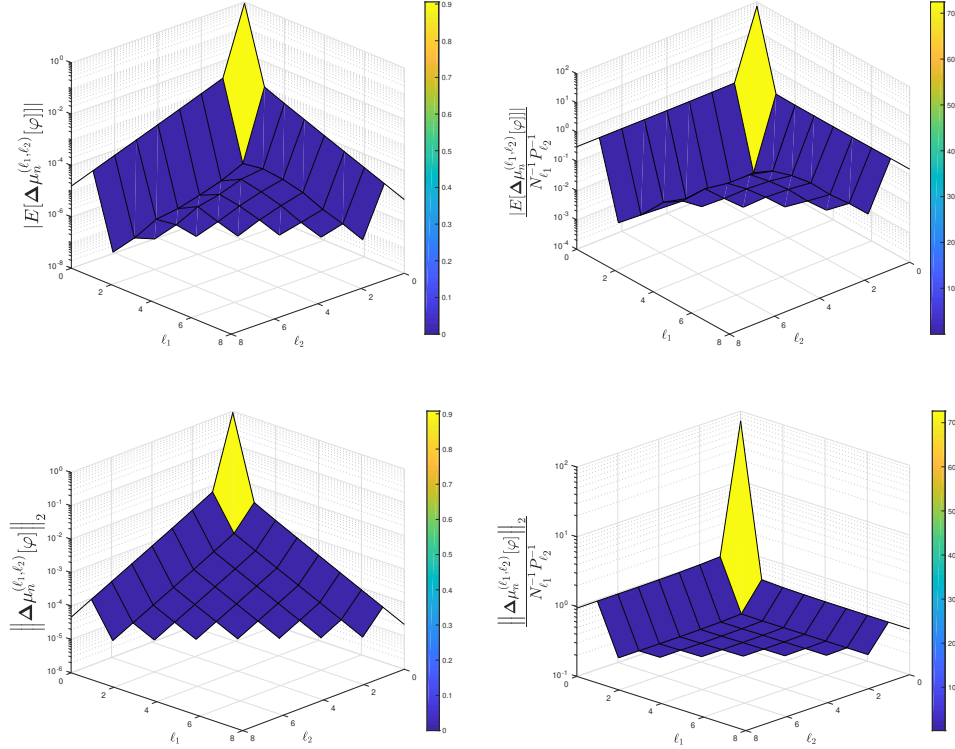


FIGURE 4. **Double Well problem. Estimates based on  $S = 10^6$  independent runs (Section 5.3).** Top row: Numerical evidence of assumption **A1** for  $\mathcal{N} = 10$  observation times when using  $N_{\ell_1} = 4 \times 2^{\ell_1}$  and  $P_{\ell_2} = 20 \times 2^{\ell_2}$ . Bottom row: Similar plots for verifying assumption **A2\***.



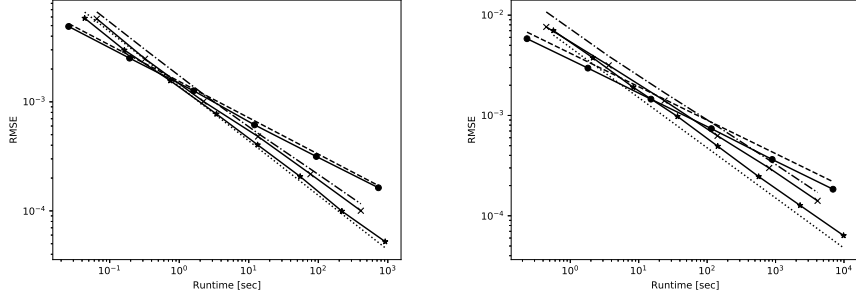


FIGURE 5. **Double Well problem. Estimates based on  $S = 100$  independent runs (Section 5.3).** Similar plots as those shown in Figure 3.

$$\text{MLEnKF: } \begin{cases} L = \lceil \log_2(\epsilon^{-1}) \rceil - 1, \\ N_\ell = 2 \times 2^\ell, \\ P_\ell = 8 \times 2^\ell, \\ M_\ell = \begin{cases} 2 \times \lceil \epsilon^{-2} L^2 2^{-2} \rceil & \text{if } \ell = 0, \\ \lceil \epsilon^{-2} L^2 2^{-2\ell-2} \rceil & \text{if } 1 \leq \ell \leq L, \end{cases} \end{cases}$$

and

$$\text{MIEnKF: } \begin{cases} L = \lceil L_* + \log_2(L_*) \rceil - 1, & \text{with } L_* = \lceil \log_2(\epsilon^{-1}) \rceil - 1 \\ N_{\ell_1} = 4 \times 2^{\ell_1}, \\ P_{\ell_2} = 20 \times 2^{\ell_2}, \\ M_\ell = \begin{cases} 6 \times \lceil \epsilon^{-2} N_{\ell_1}^{-3/2} P_{\ell_2}^{-3/2} \rceil & \text{if } \ell_1 = 0 \text{ and } \ell_2 = 0, \\ 50 \times \lceil \epsilon^{-2} N_{\ell_1}^{-3/2} P_{\ell_2}^{-3/2} \rceil & \text{if } 1 \leq \ell_1 + \ell_2 \leq L. \end{cases} \end{cases}$$

To shed some light on the importance of the temperature parameter, Figure 6 illustrates the phase-portrait time evolution of the realization of Langevin dynamics up to the final time  $\mathcal{N} = 50$  for different temperatures  $T$ . Damping causes a rapid decay of the velocity from the initial value to zero when  $T = 0$ . For positive temperatures, thermal fluctuation leads to more diffusive dynamics. Figure 7 shows the signal-tracking performance of MIEnKF for the full observation operator

$$H = \begin{bmatrix} 1 & 0 \\ 0 & 1 \end{bmatrix}$$

and the partial observation operators  $H = [1 \ 0]$  or  $H = [0 \ 1]$ , all computed at the tolerance  $\epsilon = 2^{-7}$ . The method is tracking the true state of the observed components well in all cases, but, as is to be expected, it does not track the true state of unobserved components with the same level of accuracy. The numerical verification of assumptions A1 and A2\* with respect to different observation operators is shown in Figures 8 and 9, respectively. For a sequence of predefined tolerances,  $\epsilon = [2^{-4}, 2^{-5}, \dots, 2^{-9}]$  for EnKF and MLEnKF and  $\epsilon = [2^{-4}, 2^{-5}, \dots, 2^{-10}]$  for MIEnKF, we compare the performance of the three methods in terms of runtime versus RMSE. We consider  $\mathcal{N} = 10$  and  $\mathcal{N} = 20$  observation times, the QoI  $\varphi(X, V) = X$  and  $\varphi(X, V) = V$ , and we use  $S = 90$  independent runs of each

method to estimate both RMSE and runtime. Figures 10 and 11 show the results for the observation operators

$$H = [1 \ 0] \quad \text{and} \quad H = \begin{bmatrix} 1 & 0 \\ 0 & 1 \end{bmatrix},$$

respectively. The observed complexity rates for MIEnKF are close to the theory, and the method is more efficient than the alternatives for small tolerances in both cases.

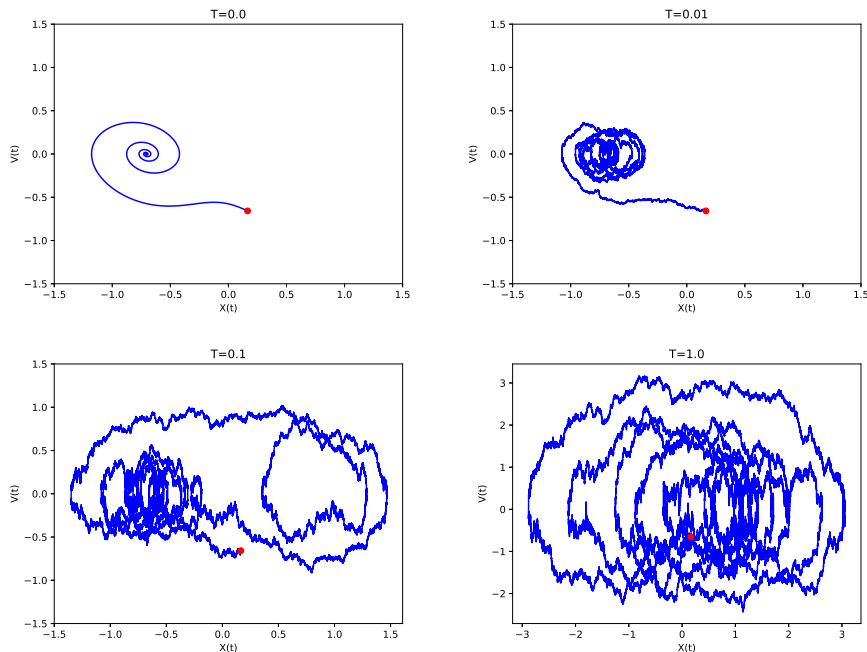


FIGURE 6. **Time evolution of a solution to Langevin dynamics with different temperature  $T$  values.** The symplectic Euler scheme is used up to final time  $\mathcal{N} = 50$ . The red dot represents the initial value.

## 6. CONCLUSION

We have developed a multi-index Monte Carlo based EnKF method, namely MIEnKF, which is based on independent samples of four-coupled EnKF estimators on a multi-index hierarchy of resolution levels. Under Assumptions 1 and 2, we proved the efficiency of the proposed method theoretically. Further, we numerically verified that this method is more efficient than MLEnKF and EnKF. A natural extension of this work is to develop MIEnKF for spatiotemporal models discretized in both space and time, e.g., stochastic partial differential equations. We believe that MIEnKF will often outperform alternative methods prominently when more than two degrees of freedom need to be discretized. Further, it will be interesting to extend the MIEnKF coupling theory to the more general “splitting parameter”/“common ratio”  $\lambda = P_{\ell_2}/P_{\ell_2-1}$  for ensemble sizes besides  $\lambda = 2$  considered in this study.

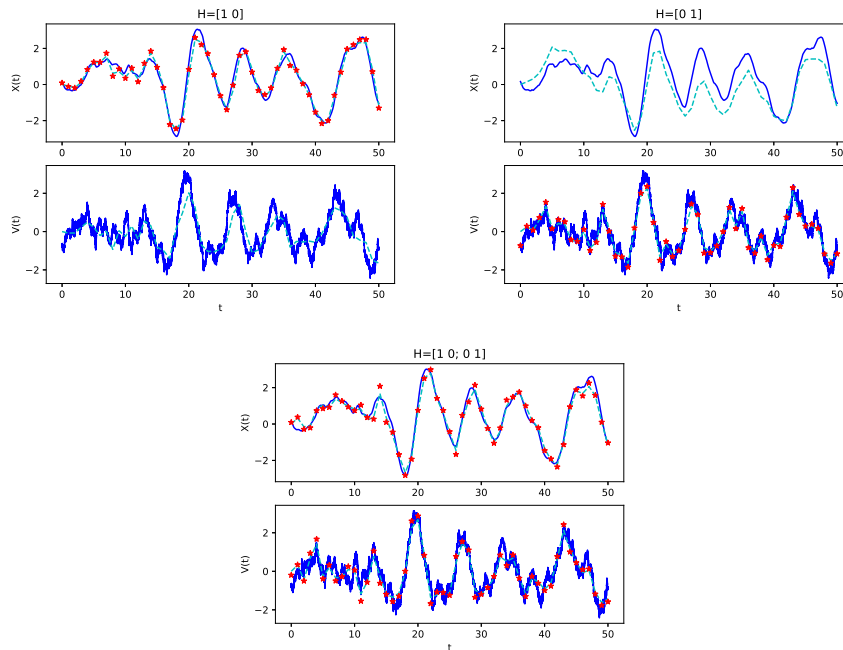


FIGURE 7. **Data assimilation for Langevin dynamics given different observation operators  $H$ , Section 5.4.** The blue solid line represents the truth, and the red stars are the observations. The cyan dashed lines represent MIEnKF mean. The final time  $\mathcal{N} = 50$  is used with the observation timestep  $\tau = 1.0$

**Acknowledgments** This work was supported by the KAUST Office of Sponsored Research (OSR) under Award No. URF/1/2584-01-01 and the Alexander von Humboldt Foundation. G. Shaimerdenova and R. Tempone are members of the KAUST SRI Center for Uncertainty Quantification in Computational Science and Engineering.

## REFERENCES

- [1] Sigurd I Aanonsen, Geir Nævdal, Dean S Oliver, Albert C Reynolds, Brice Vallès, et al. The ensemble Kalman filter in reservoir engineering—a review. *Spe Journal*, 14(03):393–412, 2009.
- [2] Mohamed Ben Alaya, Ahmed Kebaier, and Thi Bao Tram Ngo. Central Limit Theorem for the  $\sigma$ -antithetic multilevel Monte Carlo method. *arXiv preprint arXiv:2002.08834*, 2020.
- [3] Jeffrey L Anderson. An ensemble adjustment Kalman filter for data assimilation. *Monthly weather review*, 129(12):2884–2903, 2001.
- [4] Jayesh Badwaik, Nils Henrik Risebro, and Christian Klingenberg. Multilevel Monte Carlo finite volume methods for random conservation laws with discontinuous flux. *arXiv preprint arXiv:1906.08991*, 2019.
- [5] Marco Balleio, Ajay Jasra, Erik von Schwerin, and Raul Tempone. A Wasserstein coupled particle filter for multilevel estimation. *arXiv preprint arXiv:2004.03981*, 2020.
- [6] Theo Baracchini, Philip Y Chu, Jonas Šukys, Gian Lieberherr, Stefan Wunderle, Alfred Wüest, and Damien Bouffard. Data assimilation of in situ and satellite remote sensing data to 3d hydrodynamic lake models: a case study using delфт3d-flow v4. 03 and openda v2. 4. *Geoscientific Model Development*, 13(3):1267–1284, 2020.

- [7] Andrea Barth and Andreas Stein. A study of elliptic partial differential equations with jump diffusion coefficients. *SIAM/ASA Journal on Uncertainty Quantification*, 6(4):1707–1743, 2018.
- [8] Andrea Beck, Jakob Dürrwächter, Thomas Kuhn, Fabian Meyer, Claus-Dieter Munz, and Christian Rohde. hp-multilevel Monte Carlo methods for uncertainty quantification of compressible Navier–Stokes equations. *SIAM Journal on Scientific Computing*, 42(4):B1067–B1091, 2020.
- [9] Joakim Beck, Ben Mansour Dia, Luis Espath, and Raúl Tempone. Multilevel double loop Monte Carlo and stochastic collocation methods with importance sampling for Bayesian optimal experimental design. *International Journal for Numerical Methods in Engineering*, 121(15):3482–3503, 2020.
- [10] Alexandros Beskos, Ajay Jasra, Kody Law, Youssef Marzouk, and Yan Zhou. Multilevel sequential Monte Carlo with dimension-independent likelihood-informed proposals. *SIAM/ASA Journal on Uncertainty Quantification*, 6(2):762–786, 2018.
- [11] Alexandros Beskos, Ajay Jasra, Kody Law, Raul Tempone, and Yan Zhou. Multilevel sequential Monte Carlo samplers. *Stochastic Processes and their Applications*, 127(5):1417–1440, 2017.
- [12] Jeff Bezanson, Alan Edelman, Stefan Karpinski, and Viral B Shah. Julia: A fresh approach to numerical computing. *SIAM Review*, 59(1):65–98, 2017.
- [13] Craig H Bishop, Brian J Etherton, and Sharanya J Majumdar. Adaptive sampling with the ensemble transform Kalman filter. part i: Theoretical aspects. *Monthly weather review*, 129(3):420–436, 2001.
- [14] Neil K Chada, Ajay Jasra, and Fangyuan Yu. Multilevel ensemble Kalman-Bucy filters. *arXiv preprint arXiv:2011.04342*, 2020.
- [15] Alexey Chernov, Håkon Hoel, Kody JH Law, Fabio Nobile, and Raul Tempone. Multilevel ensemble Kalman filtering for spatio-temporal processes. *Numerische Mathematik*, pages 1–55, 2020.
- [16] Gianluca Detommaso, Tim Dodwell, and Rob Scheichl. Continuous level Monte Carlo and sample-adaptive model hierarchies. *SIAM/ASA Journal on Uncertainty Quantification*, 7(1):93–116, 2019.
- [17] Geir Evensen. Sequential data assimilation with a nonlinear quasi-geostrophic model using Monte Carlo methods to forecast error statistics. *Journal of Geophysical Research: Oceans*, 99(C5):10143–10162, 1994.
- [18] Wei Fang and Mike Giles. Importance sampling for pathwise sensitivity of stochastic chaotic systems. *arXiv preprint arXiv:2005.12160*, 2020.
- [19] Kristian Fossum, Trond Mannseth, and Andreas S Stordal. Assessment of multilevel ensemble-based data assimilation for reservoir history matching. *Computational Geosciences*, 24(1):217–239, 2020.
- [20] Han Gao and Jian-Xun Wang. A bi-fidelity ensemble Kalman method for pde-constrained inverse problems. *arXiv preprint arXiv:2003.11912*, 2020.
- [21] Michael B Giles. Multilevel monte carlo path simulation. *Operations research*, 56(3):607–617, 2008.
- [22] Michael B Giles and Benjamin J Waterhouse. Multilevel quasi-Monte Carlo path simulation. *Advanced Financial Modelling, Radon Series on Computational and Applied Mathematics*, 8:165–181, 2009.
- [23] Takashi Goda, Tomohiko Hironaka, and Takeru Iwamoto. Multilevel Monte Carlo estimation of expected information gains. *Stochastic Analysis and Applications*, 38(4):581–600, 2020.
- [24] Alastair Gregory and Colin J Cotter. A seamless multilevel ensemble transform particle filter. *SIAM Journal on Scientific Computing*, 39(6):A2684–A2701, 2017.
- [25] Alastair Gregory, Colin J Cotter, and Sebastian Reich. Multilevel ensemble transform particle filtering. *SIAM Journal on Scientific Computing*, 38(3):A1317–A1338, 2016.
- [26] Abdul-Lateef Haji-Ali, Fabio Nobile, and Raúl Tempone. Multi-index Monte Carlo: when sparsity meets sampling. *Numerische Mathematik*, 132(4):767–806, 2016.
- [27] Abdul-Lateef Haji-Ali and Raúl Tempone. Multilevel and multi-index Monte Carlo methods for the McKean–Vlasov equation. *Statistics and Computing*, 28(4):923–935, 2018.
- [28] Mohamad Abed El Rahman Hammoud, Issam Lakkis, Omar Knio, and Ibrahim Hoteit. Moving source identification in an uncertain marine flow: Mediterranean Sea application. *Ocean Engineering*, 220:108435, 2021.

- [29] Chiheb Ben Hammouda, Nadhir Ben Rached, and Raúl Tempone. Importance sampling for a robust and efficient multilevel Monte Carlo estimator for stochastic reaction networks. *Statistics and Computing*, 30(6):1665–1689, 2020.
- [30] Håkon Hoel and Sebastian Krumscheid. Central limit theorems for multilevel Monte Carlo methods. *Journal of Complexity*, 54:101407, 2019.
- [31] Håkon Hoel, Kody JH Law, and Raúl Tempone. Multilevel ensemble Kalman filtering. *SIAM Journal on Numerical Analysis*, 54(3):1813–1839, 2016.
- [32] Håkon Hoel, Gaukhar Shaimerdenova, and Raúl Tempone. Multilevel ensemble Kalman filtering based on a sample average of independent enkf estimators. *Foundations of Data Science*, 2(4):351, 2020.
- [33] Peter L Houtekamer and Herschel L Mitchell. Data assimilation using an ensemble Kalman filter technique. *Monthly Weather Review*, 126(3):796–811, 1998.
- [34] Peter L Houtekamer, Herschel L Mitchell, Gérard Pellerin, Mark Buehner, Martin Charron, Lubos Spacek, and Bjarne Hansen. Atmospheric data assimilation with an ensemble Kalman filter: Results with real observations. *Monthly weather review*, 133(3):604–620, 2005.
- [35] Ajay Jasra, Kengo Kamatani, Kody JH Law, and Yan Zhou. Multilevel particle filters. *SIAM Journal on Numerical Analysis*, 55(6):3068–3096, 2017.
- [36] Benjamin Jourdain, Ahmed Kebaier, et al. Non-asymptotic error bounds for the multilevel Monte Carlo euler method applied to sdes with constant diffusion coefficient. *Electronic Journal of Probability*, 24, 2019.
- [37] Eugenia Kalnay. *Atmospheric modeling, data assimilation and predictability*. Cambridge university press, 2003.
- [38] Ahmed Kebaier and Jérôme Lelong. Coupling importance sampling and multilevel Monte Carlo using sample average approximation. *Methodology and Computing in Applied Probability*, 20(2):611–641, 2018.
- [39] Amirreza Khodadadian, Maryam Parvizi, and Clemens Heitzinger. An adaptive multilevel Monte Carlo algorithm for the stochastic drift–diffusion–poisson system. *Computer Methods in Applied Mechanics and Engineering*, 368:113163, 2020.
- [40] Frances Kuo, Robert Scheichl, Christoph Schwab, Ian Sloan, and Elisabeth Ullmann. Multilevel quasi-Monte Carlo methods for lognormal diffusion problems. *Mathematics of Computation*, 86(308):2827–2860, 2017.
- [41] Jonas Latz, Iason Papaioannou, and Elisabeth Ullmann. Multilevel sequential2 Monte Carlo for Bayesian inverse problems. *Journal of Computational Physics*, 368:154–178, 2018.
- [42] François Le Gland, Valérie Monbet, and Vu-Duc Tran. *Large sample asymptotics for the ensemble Kalman filter*. PhD thesis, INRIA, 2009.
- [43] Alexander Litvinenko, Abdulkadir C Yucel, Hakan Bagci, Jesper Ooppelstrup, Eric Michielssen, and Raúl Tempone. Computation of electromagnetic fields scattered from objects with uncertain shapes using multilevel Monte Carlo method. *IEEE Journal on Multiscale and Multiphysics Computational Techniques*, 4:37–50, 2019.
- [44] Kjetil O Lye, Siddhartha Mishra, and Roberto Molinaro. A multi-level procedure for enhancing accuracy of machine learning algorithms. *arXiv preprint arXiv:1909.09448*, 2019.
- [45] Jan Mandel, Loren Cobb, and Jonathan D Beezley. On the convergence of the ensemble Kalman filter. *Applications of Mathematics*, 56(6):533–541, 2011.
- [46] Gabriel Moldovan, Guillaume Lehnasch, Laurent Cordier, and Marcello Meldi. A multi-grid/ensemble Kalman filter strategy for assimilation of unsteady flows. *arXiv preprint arXiv:2012.10091*, 2020.
- [47] Pierre Del Moral, Ajay Jasra, Kody JH Law, and Yan Zhou. Multilevel sequential Monte Carlo samplers for normalizing constants. *ACM Transactions on Modeling and Computer Simulation (TOMACS)*, 27(3):1–22, 2017.
- [48] Eike H Müller, Rob Scheichl, and Tony Shardlow. Improving multilevel Monte Carlo for stochastic differential equations with application to the Langevin equation. *Proceedings of the Royal Society A: Mathematical, Physical and Engineering Sciences*, 471(2176):20140679, 2015.
- [49] Andrey A Popov, Changhong Mou, Traian Iliescu, and Adrian Sandu. A multifidelity ensemble Kalman filter with reduced order control variates. *arXiv preprint arXiv:2007.00793*, 2020.
- [50] Andrey A Popov and Adrian Sandu. Multifidelity ensemble Kalman filtering using surrogate models defined by physics-informed autoencoders. *arXiv preprint arXiv:2102.13025*, 2021.

- [51] Pieterjan Robbe, Dirk Nuyens, and Stefan Vandewalle. Recycling samples in the multigrid multilevel (quasi-) Monte Carlo method. *SIAM Journal on Scientific Computing*, 41(5):S37–S60, 2019.
- [52] Sangeetika Ruchi, Svetlana Dubinkina, and Jana de Wiljes. Fast hybrid tempered ensemble transform filter formulation for Bayesian elliptical problems via Sinkhorn approximation. *Nonlinear Processes in Geophysics*, 28(1):23–41, 2021.
- [53] Daniel Schaden and Elisabeth Ullmann. On multilevel best linear unbiased estimators. *SIAM/ASA Journal on Uncertainty Quantification*, 8(2):601–635, 2020.
- [54] Søren Taverniers and Daniel M Tartakovsky. Estimation of distributions via multilevel Monte Carlo with stratified sampling. *Journal of Computational Physics*, 419:109572, 2020.

(Håkon Hoel)

CHAIR OF MATHEMATICS FOR UNCERTAINTY QUANTIFICATION, RWTH AACHEN UNIVERSITY, AACHEN,  
GERMANY

(HOEL@UQ.RWTH-AACHEN.DE)

(Gaukhar Shaimerdenova)

APPLIED MATHEMATICS AND COMPUTATIONAL SCIENCES, KAUST, THUWAL, SAUDI ARABIA

(GAUKHAR.SHAIMERDENOVA@KAUST.EDU.SA)

(Raul Tempone)

CHAIR OF MATHEMATICS FOR UNCERTAINTY QUANTIFICATION, RWTH AACHEN UNIVERSITY, AACHEN,  
GERMANY

(TEMPONE@UQ.RWTH-AACHEN.DE)

AND

APPLIED MATHEMATICS AND COMPUTATIONAL SCIENCES, KAUST, THUWAL, SAUDI ARABIA

(RAUL.TEMPONE@KAUST.EDU.SA)

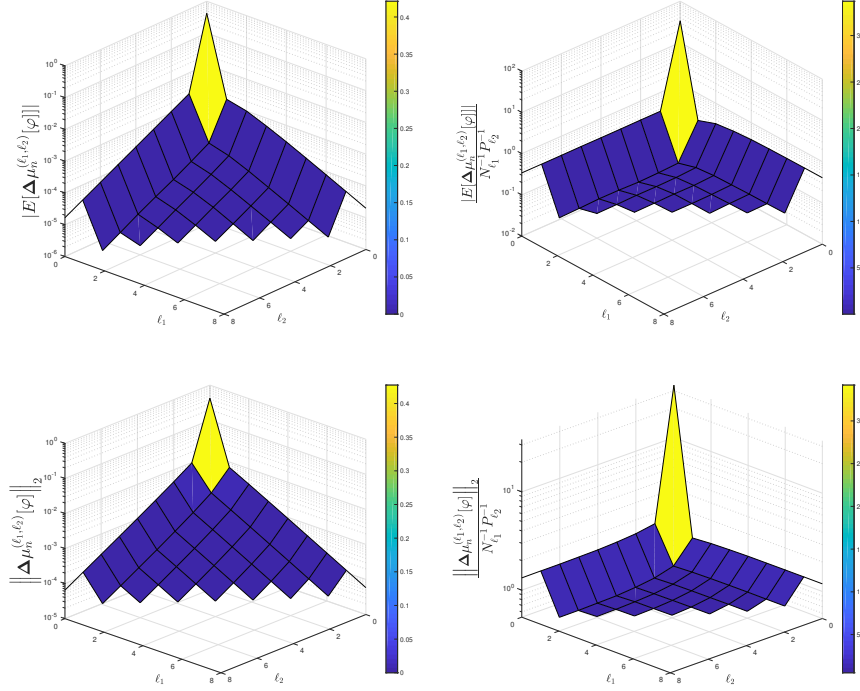
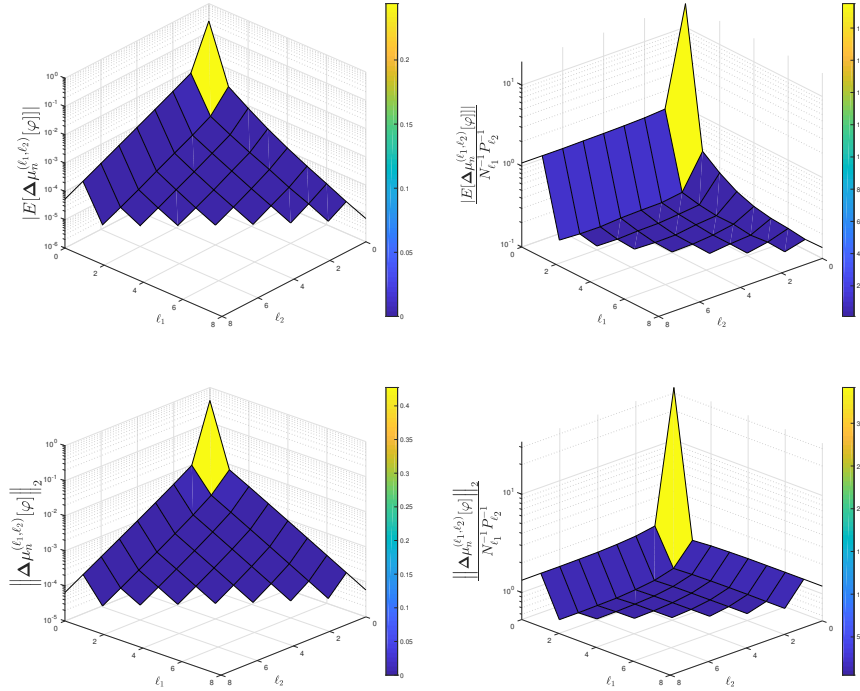
(a) The particle position  $X_t$ (b) The particle velocity  $V_t$ 

FIGURE 8. Langevin dynamics with partial observations,  $H = [1 \ 0]$ . Estimates based on  $S = 10^6$  independent runs (Section 5.4). Top row in each subfigure: Numerical evidence of assumption **A1** for  $\mathcal{N} = 10$  observation times when using  $N_{\ell_1} = 4 \times 2^{\ell_1}$  and  $P_{\ell_2} = 20 \times 2^{\ell_2}$ . Bottom row in each subfigure: Similar plots for verifying assumption **A2\***.

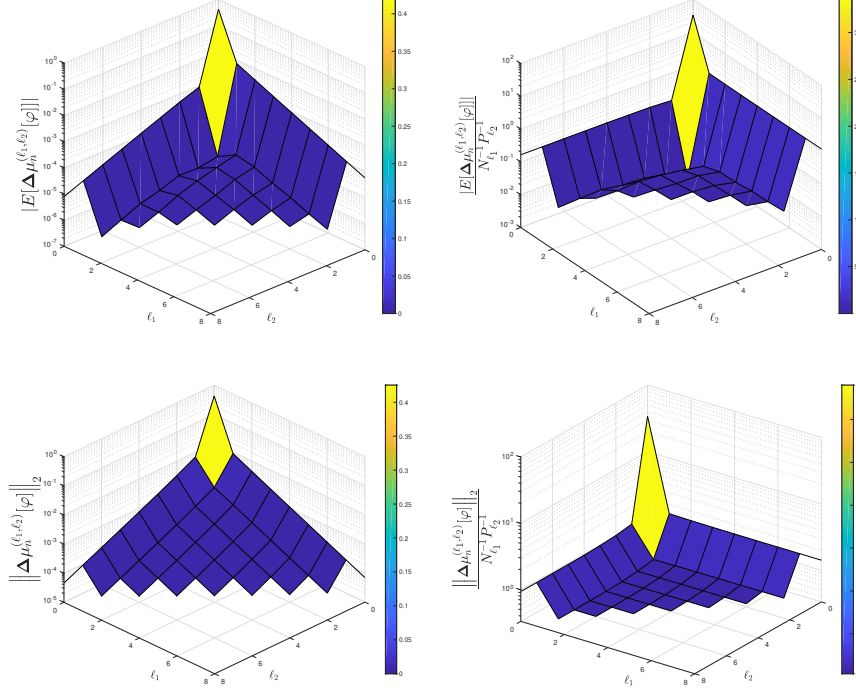
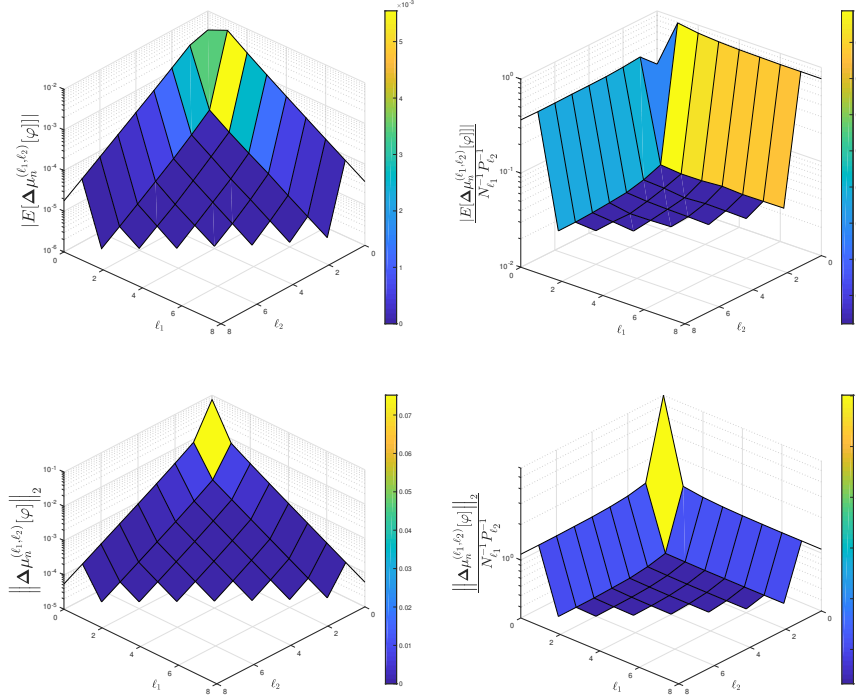
(a) The particle position  $X_t$ (b) The particle velocity  $P_t$ 

FIGURE 9. Langevin dynamics with full observations,  $H = [1 \ 0; 0 \ 1]$ . Estimates based on  $S = 10^6$  independent runs (Section 5.4). Similar plots as those shown in Figure 8.



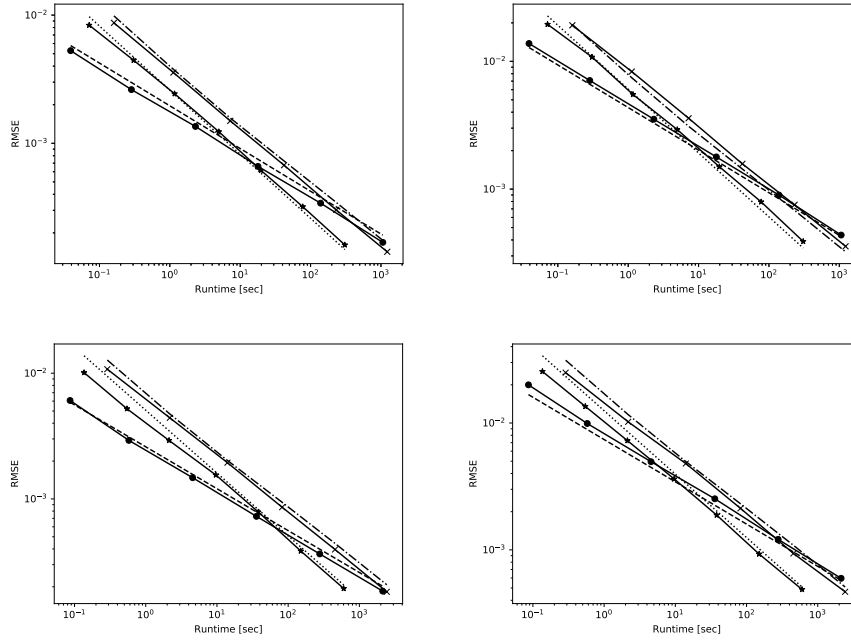


FIGURE 10. **Langevin dynamics with partial observations,  $H = [1 \ 0]$ . Estimates based on  $S = 90$  independent runs (Section 5.4).** *Top row:* Comparison of the runtime versus RMSE for the mean of the component  $X$  (left) and the component  $V$  (right) over  $\mathcal{N} = 10$  observation times. The solid-crossed line represents MLEnKF and the dot-dashed line is a fitted  $\mathcal{O}(\log(10 + \text{Runtime})^{1/3} \text{Runtime}^{-1/2})$  reference line. The solid-asterisk line represents the MIEnKF and the dotted line is a fitted  $\mathcal{O}(\text{Runtime}^{-1/2})$  reference line. The solid-bulleted line represents EnKF and the dashed line is a fitted  $\mathcal{O}(\text{Runtime}^{-1/3})$  reference line. *Bottom row:* Similar plots for  $\mathcal{N} = 20$  observation times.

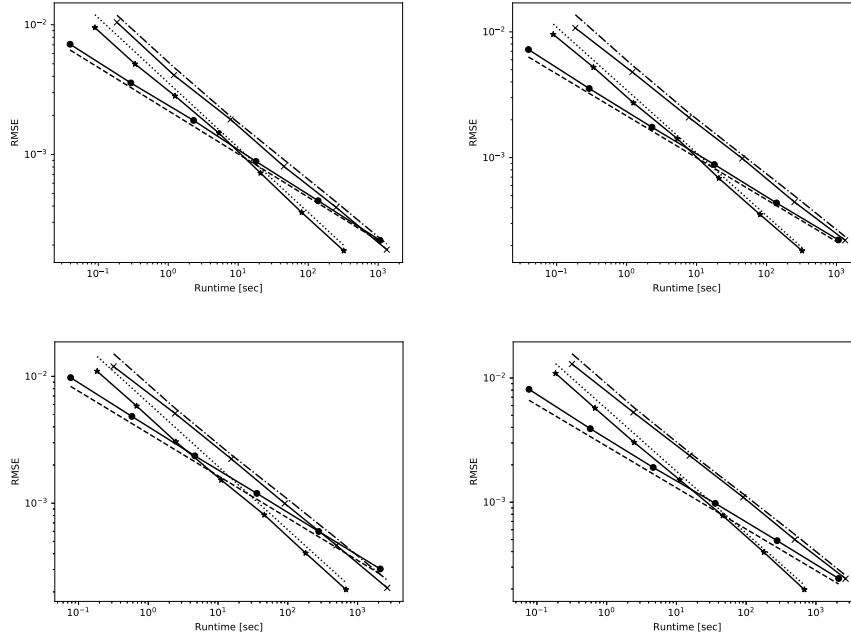


FIGURE 11. Langevin dynamics with full observations,  $H = [1 \ 0; 0 \ 1]$ . Estimates based on  $S = 90$  independent runs (Section 5.4). Similar plots as those shown in Figure 10.